Summer 2021

Buckling Loads of a Graphene Layer Interacting with Rigid Substrates

Bradley Beckwith
bgb23@uakron.edu

BUCKLING LOADS OF A GRAPHENE LAYER INTERACTING WITH RIGID SUBSTRATES

Honors Thesis

Bradley Beckwith

December 2021

Contents

1 Abstract

This project seeks to formulate a mathematical model to predict the buckling of a graphene layer between two rigid substrates. The model is designed to represent a theoretical system consisting of a graphene layer when it is parallel to the substrates and an edge load is applied to the ends of the layer. Our goal is to use this model to predict buckling loads given different assumptions for Van der Waals forces between the graphene layer and the substrates. The motivation for this project is to further our knowledge regarding the mechanical properties of graphene. The results of this project will contribute to a better theoretical understanding of graphene's deformation in response to applied loads. These developments can be applied to assist engineers and scientists in incorporating graphene into a variety of potential applications. Furthermore, this research will advance the understanding of the mechanics of nanoscale structures.

2 Introduction

Fullerenes are cage like structures formed by carbon atoms in a hexagonal lattice configuration. In the 1980's, researchers at Rice University were the first to begin investigating the chemistry of fullerenes [1]. This research laid the groundwork for the eventual identification and synthesis of carbon nanotubes, which are a longer configuration of the fullerene structure. You can think of carbon nanotubes as a sheet of graphite rolled into a tube-like cylinder.

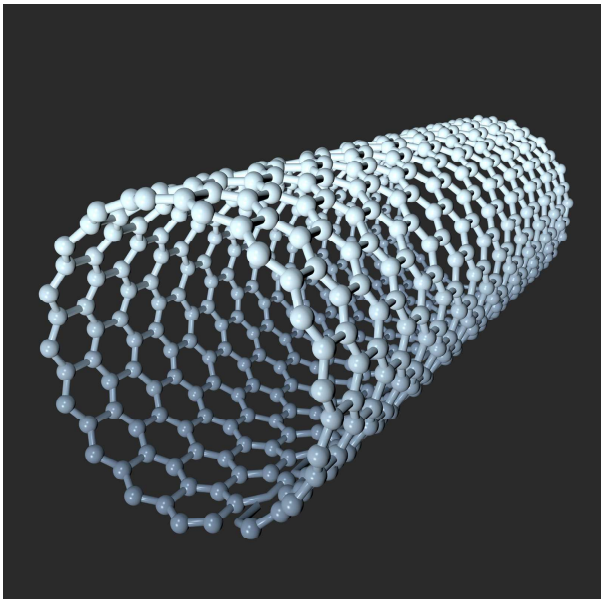

Figure 1: The geometry of a carbon nanotube [2].

Researchers first observed carbon nanotubes in 1991 using transmission electron microscopy techniques [3]. Initially, the early nanotubes observed were multi-wall nanotubes, but by 1993 researchers became more interested in single-wall nanotubes [4, 5]. As the name implies, these nanotubes consist of a single carbon layer with a wall thickness of a single atom. Due to their unique properties there was great interest in these single-wall nanotubes. Large scale synthesis techniques were eventually developed which led to widespread study and research into the many interesting properties and potential applications of the nanotubes [6, 7]. While an abundance of research now exists on this topic, there are still many questions to be answered and investigated.

Single-walled nanotubes are graphene sheets rolled into a cylindrical structure [8]. A graphene sheet is a single atom thick layer of carbon organized in a hexagonal lattice shape similar to that of a honeycomb pattern. This pattern is present in Figure 1. Because graphene sheets are the basic structure of these single-

walled nanotubes, there is value in understanding more about the properties of graphene sheets themselves [9]. By investigating graphene sheets, we can then extrapolate and apply our findings to advance the field of nanotube development and research.

Currently a large body of research exists that has observed and characterized many properties of carbon nanotubes and graphene sheets. From a mechanical perspective, researchers have discovered that carbon nanotubes have notable values of elastic strain, fracture strain sustaining capability [10, 11], and elastic modulus [12, 13] . Furthermore, dynamic simulations have been developed to illustrate the deformation properties of nanotubes. These simulations demonstrate the flexibility inherent to these nanotubes when exposed to harsh bending [14].

There has been a large amount of interest in the electrical properties of graphene for a variety of uses, some of which include nanoscale devices [15]. An abundance of research has established a relationship between the mechanical deformation of graphene and its electrical properties [16, 17, 18, 19]. Therefore, in order for graphene to be used in the development of new nanotechnologies, we need to better understand how graphene responds to applied loads and other mechanical forces [20, 21, 22]. By better understanding the mechanical deformation of graphene sheets, researchers can harness the unique electrical properties of the material to expand the use of carbon nanotubes in novel devices and applications.

While many researchers are interested in the electrical applications of graphene and carbon nanotubes, others are interested in utilizing their mechanical properties. Because of the properties briefly mentioned previously, nanotubes and graphene are exceptional candidates for use in material reinforcement. This area of research has generated new materials including polymer [23], metal, and ceramic-matrix composites [24]. Some researchers have experienced difficulty developing these new materials, as there are often unwanted interactions between the carbon component and the material being reinforced [25]. This area of research and development could be improved by an increased understanding of the thermo-mechanical properties and behavior of the material [26]. By investigating graphene's mechanical responses, our research will potentially assist in furthering the development of these composite materials.

As established by the current literature and research in this field, it is clear that understading graphene's deformation is critical to the development of new technologies. This research project investigates how graphene responds to applied loads using mathmatical modeling. The specific system modeled here involves a sheet of graphene between two substrates with applied forces on either side of the graphene sheet. See Figure 2. A model was created to represent the total energy in the graphene and substrate system.

The model was developed by assuming that the total energy of the system contains terms describing bending energy, interaction energy, inextensibility constraints, and work from applied loads. Once this was done, a 2-point boundary problem was formed from the total energy. This was done using Calculus of Variations to write the Euler-LaGrange equations. Then, we found the trivial branch for the 2-point boundary problem. The trivial branch corresponds to the graphene being an equivalent distance from the upper and lower substrates. The next step was to linearize the problem about the trivial branch. After linearizing the problem, linear algebra methods were used to get the problem into a general form that could be solved using MATLAB code. Finally, we developed MATLAB code to predict buckling loads and to perform a parametric study by varying the parameters in the interaction terms in the model. By changing the input parameter values, we can observe how buckling occurs given different interaction forces.

3 Deriving the Total Energy Equation

This section will describe the system we study and present the different assumptions for contributions to the total energy of the system. After introducing each contribution we will put these together to form the total energy used for the model.

3.1 The Problem

First we describe the physical problem. We are studying a graphene sheet between two substrates that are D distance apart. We place the origin at the same height as the lower substrate. This means that the distance from the lower substrate to the graphene sheet can be expressed as $y(s)$ and the distance from the upper substrate to the graphene sheet is $(D - y(s))$. Any point on the graphene sheet can be written as (x, y). There is a force applied to each end of the sheet. For this model we will represent these forces with equal magnitude and opposite direction which are B and $-B$. Figure 2 illustrates the situation.

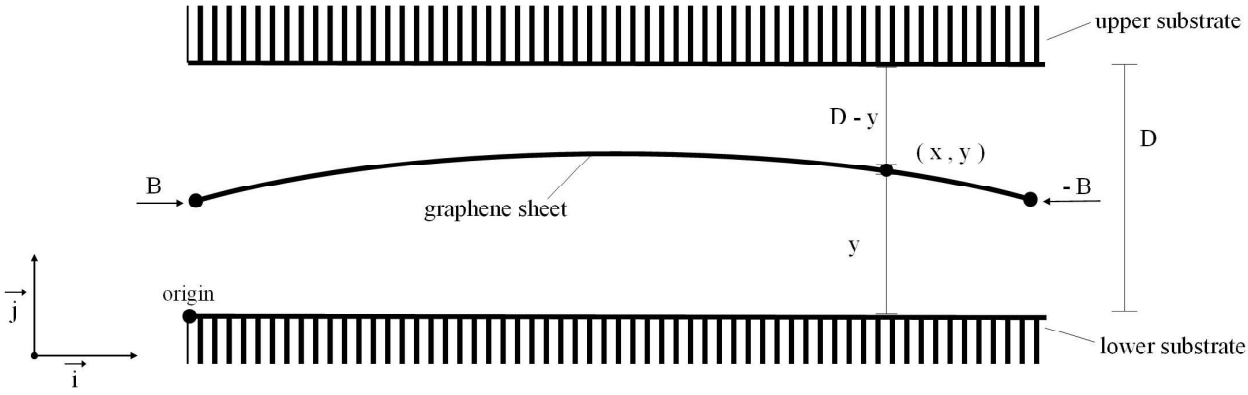

Figure 2: Geometry of a cross-section of graphene between two substrates with edge loads.

We assume that the graphene sheet deforms the same in each cross-section defined by a plane perpendicular to $\vec{k}$. We model each cross-section as a rod. Figure 2 shows a typical cross-section in the $\vec{i}\,\vec{j}$ plane. We describe a typical cross-section mathematically using a vector function

$$\vec{r}(s) = x(s)\,\vec{i} + y(s)\,\vec{j} \qquad \text{for } s \text{ in} [0, L]. \tag{1}$$

We will also assume that the rod is inextensible. This means that the length of the rod will not

change under deformation of the graphene sheet. We assume the reference configuration of the rod is the set of points $(s, 0)$ with s in $[0, L]$ along the positive x-axis. So in the reference configuration, the length between 2 points $(a, 0)$ and $(s, 0)$ is $s - a$, where we assume $a < s$. From inextensibility we also know that

$$(s-a) = \int_a^s |\vec{r}'(\xi)| d\xi,$$

which implies that

$$\frac{d}{ds}(s-a) = \frac{d}{ds}\int_a^s |\vec{r}'(\xi)| d\xi$$

or

$$1 = |\vec{r}'(s)| \,.$$

This means $\vec{r}'(s)$ lies on a unit circle and we can write $\vec{r}'(s)$ as

$$\vec{r}'(s) = \cos(\theta(s))\,\vec{i} + \sin(\theta(s))\,\vec{j}\,. \tag{2}$$

Using (1) and (2), we see that

$$x'(s) = \cos(\theta(s)),$$

$$y'(s) = \sin(\theta(s)). \tag{3}$$

3.2 Bending Energy Component

We next compute the curvature of the cross-section of the graphene sheet. Recall that the curvature κ is defined by

$$\kappa(s) = \frac{|\vec{T}'(s)|}{|\vec{r}'(s)|}.$$

We know

$$\vec{T}'(s) = \frac{\vec{r}'(s)}{|\vec{r}'(s)|} = \frac{\cos(\theta(s))\,\vec{i} + \sin(\theta(s))\,\vec{j}}{1} = \cos(\theta(s))\,\vec{i} + \sin(\theta(s))\,\vec{j}\,.$$

Hence

$$\vec{T}'(s) = -\sin(\theta)\theta' i + \cos(\theta)\theta' j$$

and

$$|\vec{T}'(s)| = |-\sin(\theta)\theta' i + \cos(\theta)\theta' j| = |\theta'|.$$

So

$$\kappa(s) = |\theta'(s)|.$$

We use θ' as the signed curvature. The bending energy for the model will be defined as

$$BE = \frac{k}{2}\int_0^L \theta'(s)^2 ds. \tag{4}$$

In this, k is the bending modulus or rigidity of the graphene represented as positive constant.

3.3 Interaction Energy

For this model there is an upper and lower substrate. We assume there is interaction between the substrates and the graphene sheet. We assume that this interaction at the point s on the cross-section depends only on the vertical distances betweeen that point and the upper and lower substrates. We let V_l and V_u denote the interaction energy per unit length with the lower and upper substrates. Hence the total interaction energy is

$$\int_0^L V_l(y(s))ds + \int_0^L V_u(D - y(s))ds. \tag{5}$$

Specific functional forms for V_l and V_u will be introduced in section 6 to evaluate the effects of interaction energy. See (53).

In the total energy, the constraint of inextensibility is enforced by introducing the terms

$$\int_0^L \gamma_1(s)(y'(s) - \sin(\theta(s)))ds + \int_0^L \gamma_2(s)(x'(s) - \cos(\theta(s)))ds. \tag{6}$$

Here γ_1 and γ_2 are LaGrange multipliers.

3.4 Work From Applied Loads

The application of the edge load displaces the ends of the cross-section meaning work is done. This causes energy to be stored in the system. This means we must subtract off the work from both edge loads. Here we will derive the work from the applied loads for each side. Work is the dot product of the force and

displacement. Hence

$$\begin{aligned} W_{left} &= \vec{F} \cdot \vec{D} \\ &= B\vec{i} \cdot (\vec{r}(0) - \vec{r}_i) \\ &= B\vec{i} \cdot (x(0) - x_l)\vec{i} + (y(0) - y_l)\vec{j}) = B(x(0) - x_l), \end{aligned}$$

and

$$W_{right} = \vec{F} \cdot \vec{D} = -B\vec{i} \cdot (\vec{r}(L) - \vec{r}_f) = -B\vec{i} \cdot (x(L) - x_r)\vec{i} + (y(L) - y_r)\vec{j}) = -B(x(L) - x_r).$$

This gives

$$W_{left} = B(x(0) - x_l) \tag{7}$$

and

$$W_{right} = -B(x(L) - x_r). \tag{8}$$

3.5 Total Energy Equation

By combining the bending energy (4), interaction energy (5), inextensibility constraints (6), and subtracting off the work from the applied loads (7, 8) we get the following equation for total energy,

$$\begin{aligned} E[x, y, \theta] = \frac{k}{2}\int_0^L \theta'(s)^2 ds + \int_0^L V_l(y(s)) + \int_0^L V_u(D - y(s)) + \int_0^L \gamma_1(s)(y'(s) - \sin(\theta(s)))ds \\ + \int_0^L \gamma_2(s)(x'(s) - \cos(\theta(s)))ds - B(x(0) - x_l) - (-B(x(L) - x_r)). \end{aligned} \tag{9}$$

4 Deriving a 2-Point Boundary-Value Problem

In this section we derive a 2-point boundary-value problem whose solutions are equilibrium configurations of the rod. For this we use standard methods of the Calculus of Variations to develop Euler-Legrange equations by seeking minimizers of the total energy. Let $(\overline{x}, \overline{y}, \overline{\theta})$ be a minimizer of the total energy E. We define a new function by fixing two of the three variables. For instance we fix θ at $\overline{\theta}$ and y at $\overline{y}$. Then we can define $f(\epsilon) = E[\overline{x} + \epsilon x, \overline{y}, \overline{\theta}]$ where x is an arbitrary function. Then $f(\epsilon)$ should be mimimzed when $\epsilon = 0$. Hence we take an ϵ derivitive of $f(\epsilon)$ and we set the resulting expression to 0. The process will be completed individually for all three variables, which yields the Euler-Legrange equations.

4.1 Variation in x

We set

$$y(s) = \overline{y}(s),$$

$$\theta(s) = \overline{\theta}(s),$$

and

$$x(s) = \overline{x}(s) + \epsilon x(s)$$

in E, giving

$$\begin{aligned} f(\epsilon) &= E[\overline{x}(s) + \epsilon x(s), \overline{y}(s), \overline{\theta}(s)] \\ &= \frac{k}{2}\int_0^L \overline{\theta}'(s)^2 ds + \int_0^L V_l(\overline{y}(s))ds + \int_0^L V_u(D - \overline{y}(s))ds \\ &\quad + \int_0^L \gamma_1(s)(\overline{y}'(s) - \sin(\overline{\theta}(s)))ds) + \int_0^L \gamma_2(s)((\overline{x}(s) + \epsilon x(s))' - \cos(\overline{\theta}(s)))ds \\ &\quad - B((\overline{x}(0) + \epsilon x(0)) - x_l) - (-B((\overline{x}(L) + \epsilon x(L)) - x_r)). \end{aligned}$$

To find the minimum of the function we set the derivative equal to 0, so

$$0 = f'(0) = \frac{d}{d\epsilon} f(\epsilon)\big|_{\epsilon=0} = \frac{d}{d\epsilon} E[(\overline{x}(s) + \epsilon x(s)), \overline{y}(s), \overline{\theta}(s)]\big|_{\epsilon=0}.$$

Since we will be taking a $\frac{d}{d\epsilon}$ derivative of each side we can remove all terms that do not have $\overline{x}(s) + \epsilon x(s)$. This leaves us with

$$
\begin{aligned}
0 &= \frac{d}{d\epsilon}\left[\int_0^L \gamma_2(s)((\overline{x}'(s) + \epsilon x'(s) - \cos(\overline{\theta}(s)))ds\right. \\
&\quad \left. -B((\overline{x}(0) + \epsilon x(0)) - x_l) - (-B((\overline{x}(L) + \epsilon x(L)) - x_r))\right]\Big|_{\epsilon=0} \\
&= \frac{d}{d\epsilon}\left[\int_0^L \gamma_2(s)((\overline{x}'(s) + \epsilon x'(s) - \cos(\overline{\theta}(s)))ds\right]\Big|_{\epsilon=0} \\
&\quad \frac{d}{d\epsilon}\left[-B((\overline{x}(0) + \epsilon x(0)) - x_l) - (-B((\overline{x}(L) + \epsilon x(L)) - x_r))\right]\Big|_{\epsilon=0} \\
&= \int_0^L \frac{d}{d\epsilon}[\gamma_2(s)\overline{x}'(s) + \gamma_2(s)\epsilon x'(s) - \gamma_2(s)\cos(\overline{\theta}(s))ds]\Big|_{\epsilon=0} \\
&\quad \frac{d}{d\epsilon}[-B((\overline{x}(0) + \epsilon x(0)) - x_l) - (-B((\overline{x}(L) + \epsilon x(L)) - x_r))]\Big|_{\epsilon=0} \\
&= \int_0^L \gamma_2(s)x'(s)ds - (Bx(0) + Bx(L)) \\
&= \gamma_2(s)x(s)\Big|_0^L - \int_0^L x(s)\gamma_2'(s)ds - B(x(0) + x(L)) \\
&= -\int_0^L x(s)\gamma_2'(s)ds + \gamma_2(s)x(s)\Big|_0^L - B(x(0) + x(L)) \\
&= -\int_0^L x(s)\gamma_2'(s)ds + \gamma_2(L)x(L) - \gamma_2(0)x(0) - Bx(0) + Bx(L)),
\end{aligned}
$$

so

$$
0 = -\int_0^L x(s)\gamma_2'(s)ds + x(L)(\gamma_2(L) + B) - x(0)(\gamma_2(0) + B). \tag{10}
$$

Because (10) must hold for arbitrary functions $x(s)$, we can conclude by standard arguments from the Calculus of Variations that

$$
\begin{aligned}
0 &= \gamma_2'(s), \\
-B &= \gamma_2(L), \\
-B &= \gamma_2(0).
\end{aligned}
$$

These three equations together imply

$$
\gamma_2 = -B. \tag{11}
$$

4.2 Variation in y

We set

$$x(s) = \overline{x}(s),$$

$$\theta(s) = \overline{\theta}(s),$$

and

$$y(s) = \overline{y}(s) + \epsilon y(s)$$

in E, giving

$$\begin{aligned} f(\epsilon) &= E[(\overline{x}(s), \overline{y}(s) + \epsilon y(s), \overline{\theta}(s)] \\ &= \frac{k}{2} \cdot \int_0^L \overline{\theta}'(s)^2 ds + \int_0^L V_l(\overline{y}(s) + \epsilon y(s)) ds + \int_0^L V_u(D - (\overline{y}(s) + \epsilon y(s))) ds \\ &\quad + \int_0^L \gamma_1(s)((\overline{y}(s) + \epsilon y(s))' - \sin(\overline{\theta}(s))) ds) + \int_0^L \gamma_2(s)(\overline{x}'(s) - \cos(\overline{\theta}(s))) ds \\ &\quad - B(\overline{x}(0) - \overline{x}_l) - (-B(\overline{x}(L) - \overline{x}_r)). \end{aligned}$$

Again, to find the minimum of the function we set the derivative equal to 0, so

$$0 = f'(0) = \frac{d}{d\epsilon} f(\epsilon)\big|_{\epsilon=0} = \frac{d}{d\epsilon} E[\overline{x}(s), \overline{y}(s) + \epsilon y(s), \overline{\theta}(s)]\big|_{\epsilon=0}.$$

Since we will be taking a $\frac{d}{d\epsilon}$ derivative of each side we can remove all terms that do not have $\overline{y}(s) + \epsilon y(s)$. This leaves us with

$$\begin{aligned} 0 &= \frac{d}{d\epsilon} \left[\int_0^L V_l(\overline{y}(s) + \epsilon y(s)) ds + \int_0^L V_u(D - (\overline{y}(s) + \epsilon y(s))) ds \right. \\ &\quad \left. + \int_0^L \gamma_1(s)((\overline{y}(s) + \epsilon y(s))' - \sin(\overline{\theta}(s))) ds) \right] \big|_{\epsilon=0} \\ &= \frac{d}{d\epsilon} \left[\int_0^L V_l(\overline{y}(s) + \epsilon y(s)) ds + V_u(D - (\overline{y}(s) + \epsilon y(s))) ds \right] \big|_{\epsilon=0} \\ &\quad + \frac{d}{d\epsilon} \left[\int_0^L \gamma_1(s)((\overline{y}(s) + \epsilon y(s))' - \sin(\overline{\theta}(s))) ds) \right] \big|_{\epsilon=0} \end{aligned}$$

$$
\begin{aligned}
&= \int_0^L \frac{d}{d\epsilon}\left[V_l(\overline{y}(s)+\epsilon y(s))ds + V_u(D-(\overline{y}(s)+\epsilon y(s)))\right] ds\Big|_{\epsilon=0} \\
&\quad + \int_0^L \frac{d}{d\epsilon}[\gamma_1(s)\overline{y}'(s) + \gamma_1(s)\epsilon y'(s) - \gamma_1(s)\sin(\overline{\theta}(s))]ds\Big|_{\epsilon=0} \\
&= \int_0^L [V_l'(\overline{y}(s)+\epsilon y(s))y(s)ds - V_u'(D-(\overline{y}(s)+\epsilon y(s)))y(s)]ds\Big|_{\epsilon=0} \\
&\quad + \int_0^L [\gamma_1(s)y'(s)ds]\Big|_{\epsilon=0} \\
&= \int_0^L [V_l'(\overline{y}(s))y(s) - V_u'(D-(\overline{y}(s)))y(s)]ds - \int_0^L \gamma_1'(s)y(s)ds + \gamma_1(s)y(s)\Big|_0^L \\
&= \int_0^L [V_l'(\overline{y}(s))y(s) - V_u'(D-(\overline{y}(s)))y(s) - \gamma_1'(s)y(s)ds] + \gamma_1(L)y(L) - \gamma_1(0)y(0)
\end{aligned}
$$

so

$$
0 = \int_0^L y(s)[V_l'(\overline{y}(s)) - V_u'(D-\overline{y}(s)) - \gamma_1'(s)]ds + \gamma_1(L)y(L) - \gamma_1(0)y(0). \tag{12}
$$

Because (12) must hold for arbitrary functions $y(s)$, we can conclude by standard arguments from the Calculus of Variations that

$$
\gamma_1'(s) = V_l'(\overline{y}(s)) - V_u'(D-(\overline{y}(s))), \tag{13}
$$

$$
0 = \gamma_1(L), \tag{14}
$$

$$
0 = \gamma_1(0). \tag{15}
$$

4.3 Variation in θ

We set

$$
x(s) = \overline{x}(s),
$$

$$
y(s) = \overline{y}(s),
$$

and

$$
\theta(s) = \overline{\theta}(s) + \epsilon\theta(s)
$$

in E, giving

$$
f(\epsilon) = E[(\overline{x}(s), \overline{y}(s), \overline{\theta}(s) + \epsilon\theta(s)]
$$

$$
\begin{aligned}
&= \frac{k}{2}\int_0^L (\overline{\theta}(s)+\epsilon\theta(s))'^2 ds + \int_0^L V_l(\overline{y}(s))ds + \int_0^L V_u(D-\overline{y}(s))ds \\
&\quad + \int_0^L \gamma_1(s)(\overline{y}'(s) - \sin(\overline{\theta}(s)+\epsilon\theta(s)))ds + \int_0^L \gamma_2(s)(\overline{x}'(s) - \cos(\overline{\theta}(s)+\epsilon\theta(s)))ds \\
&\quad - B(\overline{x}(0)-\overline{x}_l)\text{–}(-B(\overline{x}(L)-\overline{x}_r)).
\end{aligned}
$$

Again, to find the minimum of the function we set the derivative equal to 0, so

$$
0 = f'(0) = \frac{d}{d\epsilon} f(\epsilon)\big|_{\epsilon=0} = \frac{d}{d\epsilon} E[\overline{x}(s), \overline{y}(s), \overline{\theta}(s)+\epsilon\theta(s))]\big|_{\epsilon=0}.
$$

Since we will be taking a $\frac{d}{d\epsilon}$ derivative of each side we can remove all terms that do not have $\overline{\theta}(s)+\epsilon\theta(s)$. This leaves us with

$$
\begin{aligned}
0 &= \frac{d}{d\epsilon}\left[\frac{k}{2}\int_0^L (\overline{\theta}(s)+\epsilon\theta(s))'^2 ds + \int_0^L \gamma_1(s)(\overline{y}'(s) - \sin(\overline{\theta}(s)+\epsilon\theta(s)))ds \right. \\
&\quad \left. + \int_0^L \gamma_2(s)(\overline{x}'(s) - \cos(\overline{\theta}(s)+\epsilon\theta(s)))ds\right]\big|_{\epsilon=0} \\
&= \int_0^L [\frac{k}{2} 2(\overline{\theta}'(s)+\epsilon\theta'(s))\theta'(s) - \gamma_1(s)\cos(\overline{\theta}(s)+\epsilon\theta(s))\theta(s) \\
&\quad + \gamma_2(s)\sin(\overline{\theta}(s)+\epsilon\theta(s))\theta(s)]ds\big|_{\epsilon=0} \\
&= \int_0^L k\overline{\theta}'(s)\theta'(s)ds + \int_0^L [-\gamma_1(s)\cos(\overline{\theta}(s))\theta(s) + \gamma_2(s)\sin(\overline{\theta}(s))\theta(s)]ds \\
&= k\overline{\theta}'(s)\theta(s)\big|_0^L - \int_0^L k\overline{\theta}''(s)\theta(s)ds + \int_0^L [-\gamma_1(s)\cos(\overline{\theta}(s))\theta(s) + \gamma_2(s)\sin(\overline{\theta}(s))\theta(s)]ds
\end{aligned}
$$

$$
0 = k\overline{\theta}'(L)\theta(L) - k\overline{\theta}'(0)\theta(0) + \int_0^L \theta(s)(-k\overline{\theta}''(s) - \gamma_1(s)\cos(\overline{\theta}(s)) + \gamma_2(s)\sin(\overline{\theta}(s)))ds. \tag{16}
$$

Because (16) must hold for arbitrary functions $\theta(s)$, we can conclude by standard arguments from the Calculus of Variations that

$$
0 = -k\overline{\theta}''(s) - \gamma_1(s)\cos(\overline{\theta}(s)) + \gamma_2(s)\sin(\overline{\theta}(s)), \tag{17}
$$

$$0 = k\overline{\theta}'(L),$$

$$0 = k\overline{\theta}'(0).$$

Rearranging (17) and substituting $\gamma_2(s)$ with -B (see (11)) gives

$$\overline{\theta}''(s) = -\frac{\gamma_1(s)}{k}\cos(\overline{\theta}(s)) - \frac{B}{k}\sin(\overline{\theta}(s)), \tag{18}$$

$$0 = \overline{\theta}'(L), \tag{19}$$

$$0 = \overline{\theta}'(0). \tag{20}$$

5 Identifying the 2-Point Boundary Problem

In this section we identify the 2-point boundary problem from the equations in the previous sections as well as nondimensionalize the problem. Using (3), (13), (14), (15), (18), (19), and (20) we can identify

$$\begin{aligned}
\hat{y}'(s) &= \sin(\hat{\theta}(s)),\\
\gamma_1'(s) &= V_l'(\overline{y}(s)) - V_u'(D - (\overline{y}(s))),\\
\overline{\theta}''(s) &= -\frac{\gamma_1(s)}{k}\cos(\overline{\theta}(s)) - \frac{B}{k}\sin(\overline{\theta}(s)),
\end{aligned}$$

with boundary conditions

$$\begin{aligned}
0 &= \gamma_1(L) = \gamma_1(0),\\
0 &= \overline{\theta}'(L) = \overline{\theta}'(0),
\end{aligned}$$

as a 2-point boundary problem satisfied by minimizers of the total energy. From this point on we will refer to $\overline{x}(s), \overline{y}(s), \overline{\theta}(s)$ as $x(s), y(s), \theta(s)$ for easier syntax. We can convert the problem into a 1^{st}-order system of differential equations by introducting a new variable ν. Setting

$$\theta'(s) = \nu(s) \tag{21}$$

and taking a derivitive gives us

$$\theta''(s) = \nu'(s). \tag{22}$$

Adding (21) to the system and using (22) to substitute results in

$$y'(s) = \sin(\theta(s)), \tag{23}$$

$$\gamma_1'(s) = V_l'(y(s)) - V_u'(D - (y(s))), \tag{24}$$

$$\nu'(s) = -\frac{\gamma_1(s)}{k}\cos(\theta(s)) - \frac{B}{k}\sin(\theta(s)), \tag{25}$$

$$\theta'(s) = \nu(s), \tag{26}$$

with boundary conditions

$$0 = \gamma_1(L) = \gamma_1(0), 0 = \nu(L) = \nu(0). \tag{27}$$

5.1 Nondimensionalizing the 2-Point Boundary Problem

We nondimensionalize the system (23), (24), (25), (26), and (27). This will be done by introducing the non-dimensional quantities

$$\hat{s} = \frac{s}{L} \to s = \hat{s}L, \tag{28}$$

$$\hat{y} = \frac{y}{L} \to y = \hat{y}L, \tag{29}$$

$$\hat{\nu} = \nu L \to \nu = \frac{\hat{\nu}}{L}, \tag{30}$$

$$\hat{D} = \frac{D}{L} \to D = \hat{D}L, \tag{31}$$

$$\hat{\theta} = \theta \to \theta = \hat{\theta} \tag{32}$$

$$\hat{\gamma_1} = \frac{\gamma_1 L^2}{k} \to \gamma_1 = \frac{\hat{\gamma_1} k}{L^2}, \tag{33}$$

and

$$\hat{B} = \frac{BL^2}{k} \to B = \frac{\hat{B}k}{L^2}. \tag{34}$$

It is also necessary to relate the derivitives for the variables. These relations are

$$y' = \frac{dy}{ds} = \frac{d(\hat{y}L)}{d(\hat{s}L)} = \frac{L}{L}\frac{d\hat{y}}{d\hat{s}} = \frac{d\hat{y}}{d\hat{s}}, \tag{35}$$

$$\nu' = \frac{d\nu}{ds} = \frac{d(\hat{\nu}\frac{1}{L})}{d(\hat{s}L)} = \frac{1}{L^2}\frac{d\hat{\nu}}{d\hat{s}}, \tag{36}$$

$$\theta' = \frac{d\theta}{ds} = \frac{d(\hat{\theta})}{d(\hat{s}L)} = \frac{1}{L}\frac{d\hat{\theta}}{d\hat{s}}, \tag{37}$$

and

$$\gamma_1' = \frac{d\gamma_1}{ds} = \frac{(\hat{\gamma_1}\frac{k}{L^2})}{d(\hat{s}L)} = \frac{k}{L^3}\frac{d\hat{\gamma_1}}{d\hat{s}}. \tag{38}$$

We substitute (35) and (32) into (23) to get

$$\frac{d\hat{y}}{d\hat{s}} = \sin(\hat{\theta}). \tag{39}$$

Substituting (37) and (30) into (26) gives

$$\frac{1}{L}\frac{d\hat{\theta}}{d\hat{s}} = \frac{\hat{\nu}}{L} \rightarrow \frac{d\hat{\theta}}{d\hat{s}} = \hat{\nu}. \tag{40}$$

Substituting (36), (33), (32), and (34) into (25) gives

$$\frac{1}{L^2}\frac{d\hat{\nu}}{d\hat{s}} = \frac{-\hat{\gamma_1}\frac{k}{L^2}}{k}\cos(\hat{\theta}) - \frac{\hat{B}\frac{k}{L^2}}{k}\sin(\hat{\theta}).$$

This can be simplified to

$$\frac{d\hat{\nu}}{d\hat{s}} = -\hat{\gamma_1}\cos(\hat{\theta}) - \hat{B}\sin(\hat{\theta}). \tag{41}$$

Substituting (38), (31), and (29) into (24) gives

$$\frac{k}{L^3}\frac{d\hat{\gamma_1}}{d\hat{s}} = V_l'(\hat{y}L) - V_u'(\hat{D}L - \hat{y}L).$$

This can be simplified to

$$\frac{d\hat{\gamma_1}}{d\hat{s}} = \frac{L^3}{\kappa}V_l'(\hat{y}L) - \frac{L^3}{k}V_u'(L(\hat{D} - \hat{y})).$$

We will define two new functions, $F_l(\hat{y})$ and $F_U(\hat{y})$, as

$$F_l(\hat{y}) = \frac{L^3}{k}V_l'(\hat{y}L),$$
$$F_u(\hat{y}) = \frac{L^3}{k}V_u'(\hat{y}L).$$

Now we can write

$$\frac{d\hat{\gamma_1}}{d\hat{s}} = F_l(\hat{y}) - F_u(\hat{D} - \hat{y}). \tag{42}$$

Finally, we can substitute our boundary conditions using (33) and (30) to get

$$0 = \hat{\gamma_1}(0) = \hat{\gamma_1}(1), \quad 0 = \hat{\nu}(0) = \hat{\nu}(1). \tag{43}$$

Since we rescaled s by L, we now have boundaries at 0 and 1 instead of 0 and L.

From this point on we will replace $\hat{y}, \hat{\nu}, \hat{D}, \hat{\theta}, \hat{\gamma_1}$, and $\hat{B}$ with $y, \nu, D, \theta, \gamma_1$, and B for easier syntax. Using (39), (40), (41), (42), and (43) the nondimensionalized system is

$$\theta'(s) = \nu, \tag{44}$$

$$\nu' = -\gamma_1 \cos(\theta) - B \sin(\theta), \tag{45}$$

$$\gamma_1 = F_l(y) - F_u(D - y), \tag{46}$$

$$y' = \sin(\theta), \tag{47}$$

with boundary conditions

$$0 = \gamma_1(0) = \gamma_1(1), \quad 0 = \nu(0) = \nu(1). \tag{48}$$

The (44) through (48) 2-point boundary problem will be the problem we study for this project.

6 Identifying the Base State

In this section we identify base states for our 2-point boundary problem. We seek base states that correspond to the cross-section of the graphene sheet remaining straight and being parallel to both substrates. Hence we assume that $y(s) = \overline{y}$ for all s in $[0, 1]$ where $\overline{y}$ is a constant between 0 and D, plugging $\overline{y}$ into (47) gives

$$0 = \sin\theta,$$

hence we can choose θ to be

$$\theta = 0. \tag{49}$$

Plugging (49) into (44) gives

$$0 = \nu. \tag{50}$$

Plugging (49) and (50) into (45) gives

$$0 = -\gamma_1 \cos(0) - B\sin(0),$$

hence

$$0 = \gamma. \tag{51}$$

Plugging (51) and $\overline{y}$ into (46) gives

$$0 = F_l(\overline{y}) - F_u(D - \overline{y}). \tag{52}$$

We now make more specific assumptions about the interaction forces. To find values of $\overline{y}$ that satisfy (52), we define F_l and F_u as

$$F_l(y) = w_1\left(\left(\frac{\sigma_1}{y}\right)^{n_1} - \left(\frac{\sigma_1}{y}\right)^{n_2}\right) \text{ and } F_u(y) = w_2\left(\left(\frac{\sigma_2}{y}\right)^{n_3} - \left(\frac{\sigma_2}{y}\right)^{n_4}\right). \tag{53}$$

These definitions of F_l and F_u follow from assuming a generalization of the Lennard-Jones potential for the interaction energy between the rod and the substrate [27]. The standard Lennard-Jones potential would lead to exponents of 13 and 7 in the interaction force, which we have generalized to n_1 and n_2 in F_l and n_3 and n_4 in F_u. In our definition of F_l in (53), w_1 determines the strength of the interaction and σ_1 is the

equilibrium spacing. We will refer to w_1 as the van der Waals strength for F_l. Similar statements apply to F_u. For our parametric study in section 9, we make specific choices for n_1, n_2, n_3, and n_4. But we assume that $n_1 > n_2$ and $n_3 > n_4$, so that F_l and F_u are qualitatively similar to the interaction force we get using the standard Lennard-Jones exponent. See Figure 3. From Figure 3 we see that $F_l(1)$ is zero and that $y = \sigma_1 = 1$ is the unique equilibrium of y. We see that for $y < 1$, the interaction force is repulsive and that this repulsive force goes to infinty as y goes to 0. For $y > 1$, the interaction force is attractive. F_l has a unique minimum at $y = \sigma_1(\frac{n2}{n1})^{\frac{1}{n_2-n_1}} = 1(\frac{2}{4})^{\frac{1}{2-4}} \approx 1.4142$ and the attractive force decays to 0 as y goes to infinity.

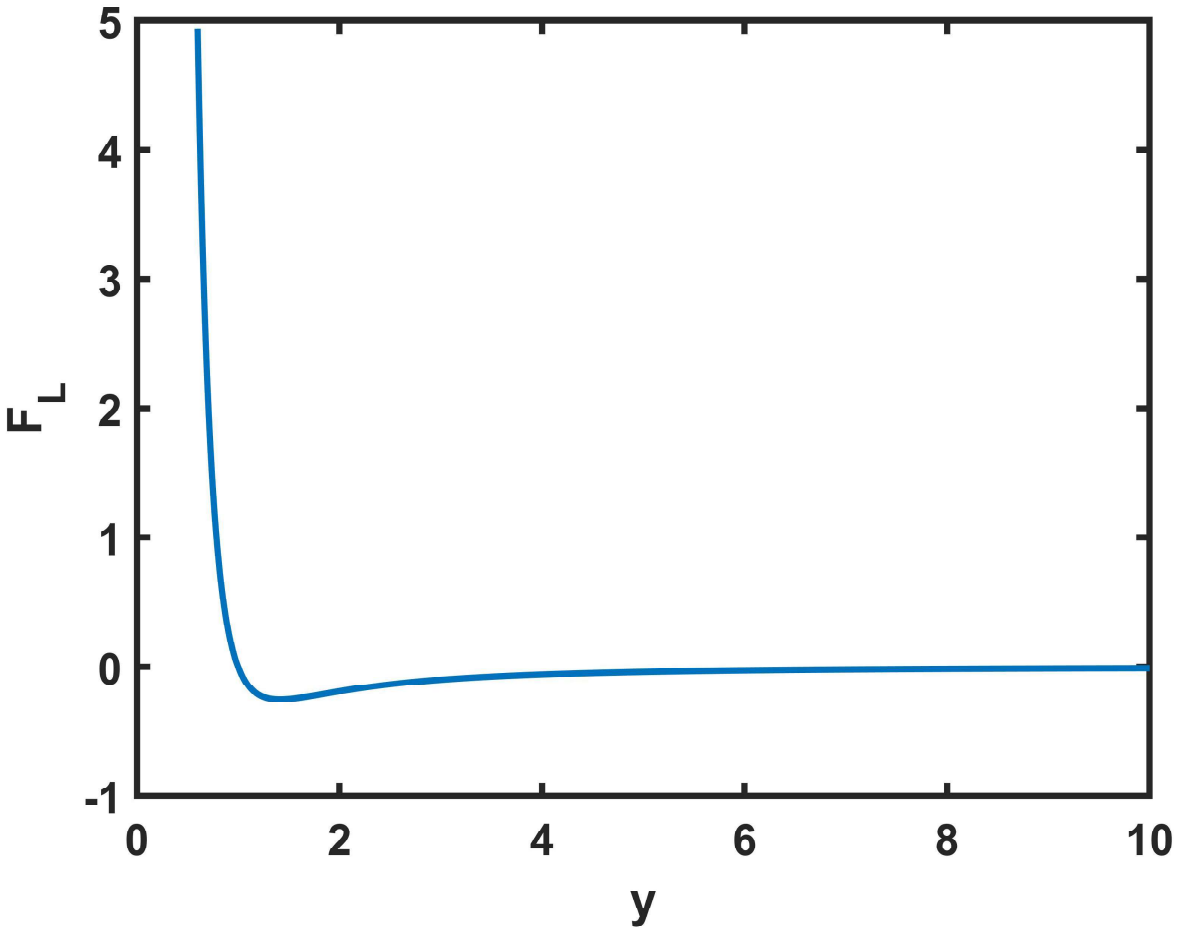

Figure 3: Lower interaction force F_l with parameters $w_1 = 1, \sigma_1 = 1, n_1 = 4$, and $n_2 = 2$.

Using (53), we can choose values for $w_1, w_2, \sigma_1, \sigma_2, n_1, n_2, n_3$, and n_4,and then we can solve (52) numerically using MATLAB. A typical such plot is shown in Figure 4.

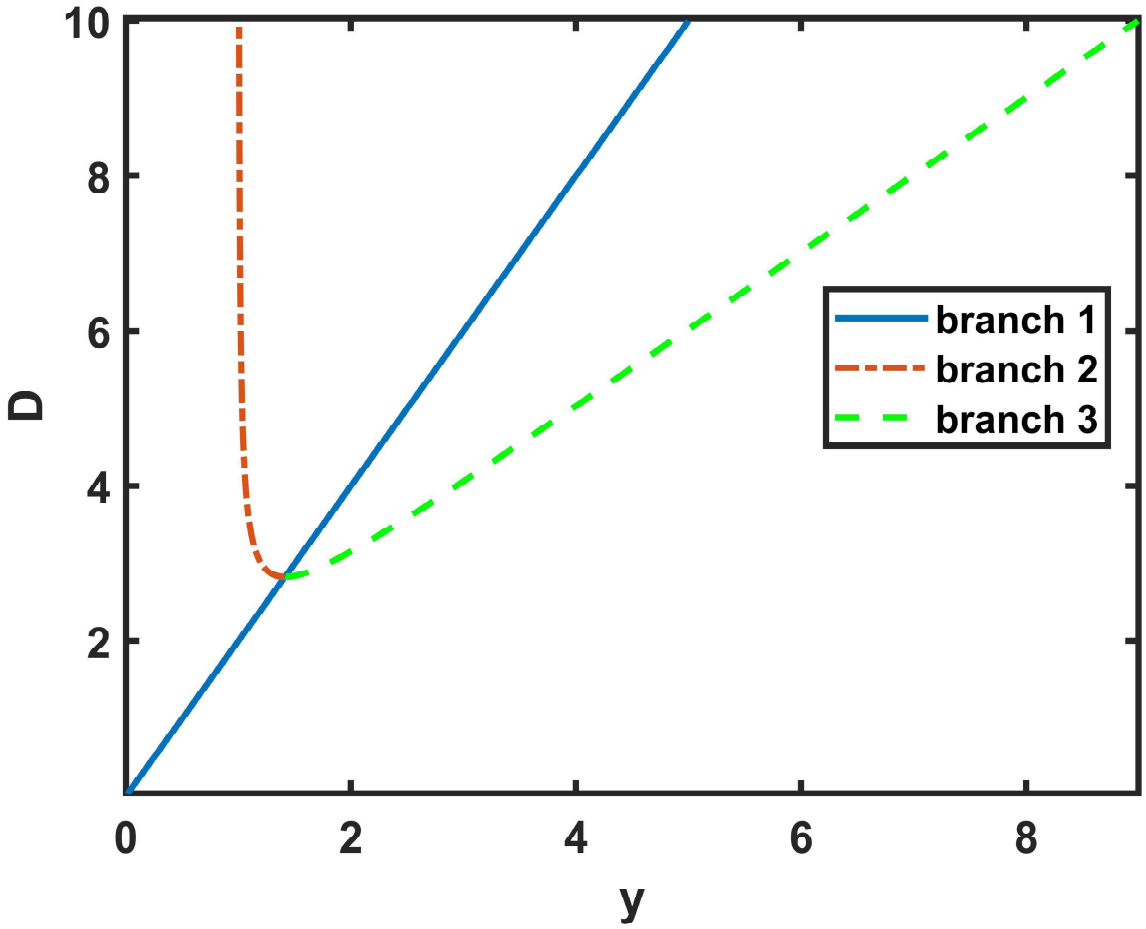

Figure 4: Equilirium configurations for $F_l = F_u$, with $w_1 = w_2 = 1, \sigma_1 = \sigma_2 = 1, n_1 = n_3 = 4$, and $n_2 = n_4 = 2$.

There are a few observations we can make about the solution curves in Figure 4 before we change the parameters. The first observation we can make is that when $F_l = F_u$, we get three different branches of equilibrium configurations. We first discuss branch 1. Here we can see that $y = \frac{1}{2}D$. This means that the rod is at equilibrium exactly halfway between the upper and lower substrates.

Next we identify the point in Figure 4 at which branches 2 and 3 split from branch 1. The y coordinate of this point can be determined to be $y = \sigma_1(\frac{n_1}{n_2})^{\frac{1}{n_1-n_2}}$. We determine this by setting $D = 2\overline{y}$ in (52), taking a derivitive of the right-hand side with respect to $\overline{y}$ setting the result to 0, and then solving for $\overline{y}$. This procedure is based on the Implicit Function Theorem. Because the point lies on the line $y = \frac{1}{2}D$, we know $D = 2\sigma_1(\frac{n_1}{n_2})^{\frac{1}{n_1-n_2}}$. We shall refer to the point $\left(\sigma_1(\frac{n_1}{n_2})^{\frac{1}{n_1-n_2}}, 2\sigma_1(\frac{n_1}{n_2})^{\frac{1}{n_1-n_2}}\right)$ as the branch point.

In Figure 4 the base state correspond to the different colored lines labeled branch 1, branch 2, and

branch 3. In section 9 we will consider different choices for the parameters in F_l and F_u when performing our parametric study of buckling.

In Figure 4, as the substrate separation increases branch 3 approaches the line $y = D - 1$. In our system, this represent the rod sticking to the upper substrate as the two substrates get further and further apart. As the separation increases, branch 2 approaches the line $y = 1$. This represent the rod sticking to the lower substrate as the substrates separate.

We can also make observations from these plots about the number of different configuration at different substrate separations. We see below the branch point in Figure 4 there is one configuration, the configuration exactly halfway between the substrates. While above the branch point there are three different configurations. It is also important to identify that in Figure 4 every value of y will have a corresponding D value that solves (52). This means at any rod height there is at least one equilibrium configuration with some substrate seperation.

6.1 Linearizing About the Base State

To linearize about the base state we will use

$$\nu = \overline{\nu} + \epsilon\hat{\nu} \qquad \text{where } \overline{\nu} = 0, \tag{54}$$

$$\theta = \overline{\theta} + \epsilon\hat{\theta} \qquad \text{where } \overline{\theta} = 0, \tag{55}$$

$$\gamma_1 = \overline{\gamma}_1 + \epsilon\hat{\gamma}_1 \qquad \text{where } \overline{\gamma}_1 = 0, \tag{56}$$

and

$$y = \overline{y} + \epsilon\hat{y} \qquad \text{where } \overline{y} = \overline{y}. \tag{57}$$

After substituting these into the system of differential equations we will take an ϵ derivitive of each and then set $\epsilon = 0$.

Substituting (55) and (54) into (44) and taking $\frac{d}{d\epsilon}$ gives

$$\frac{d}{d\epsilon}\left[\overline{\theta}' + \epsilon\hat{\theta}'\right]\Big|_{\epsilon=0} = \frac{d}{d\epsilon}\left[\overline{\nu} + \epsilon\hat{\nu}\right]\Big|_{\epsilon=0},$$

which simplifies to

$$\hat{\theta}' = \hat{\nu}. \tag{58}$$

Substituting (54), (55), and (56) into (45) and taking $\frac{d}{d\epsilon}$ gives

$$\frac{d}{d\epsilon}\left[\overline{\nu}' + \epsilon\hat{\nu}'\right]\Big|_{\epsilon=0} = \frac{d}{d\epsilon}\left[-(\overline{\gamma}_1 + \epsilon\hat{\gamma}_1)\cos(\overline{\theta} + \epsilon\hat{\theta}) - B\sin(\overline{\theta} + \epsilon\hat{\theta})\right]\Big|_{\epsilon=0},$$

$$\hat{\nu}' = -\hat{\gamma}_1\cos(0) + \sin(0)\hat{\theta}0 - B\cos(0)\hat{\theta},$$

which simplifies to

$$\hat{\nu}' = -\hat{\gamma_1} - B\hat{\theta}. \tag{59}$$

Substituting (56) and (57) into (46) and taking $\frac{d}{d\epsilon}$ gives

$$\frac{d}{d\epsilon}\left[\overline{\gamma}_1' + \epsilon\hat{\gamma_1}'\right]\Big|_{\epsilon=0} = \frac{d}{d\epsilon}\left[F_l(\overline{y} + \epsilon\hat{y}) - F_u(D - \overline{y} - \epsilon\hat{y})\right]\Big|_{\epsilon=0},$$

$$\hat{\gamma}_1' = F_l'(\overline{y})\hat{y} - F_u'(D - \overline{y})(-\hat{y}),$$

which simplifies to

$$\hat{\gamma}_1' = \hat{y}(F_l'(\overline{y}) + F_u'(D - \overline{y})).$$

We will now set

$$A = F_l'(\overline{y}) + F_u'(D - \overline{y}) \tag{60}$$

giving

$$\hat{\gamma}_1' = A\hat{y}. \tag{61}$$

Substituting (57) and (55) into (47) and taking $\frac{d}{d\epsilon}$ gives

$$\frac{d}{d\epsilon}\left[\overline{y}' + \epsilon\hat{y}'\right]\Big|_{\epsilon=0} = \frac{d}{d\epsilon}\left[\sin(\overline{\theta} + \epsilon\hat{\theta})\right]\Big|_{\epsilon=0},$$

$$\hat{y}' = \cos(0)\hat{\theta},$$

which simplifies to

$$\hat{y}' = \hat{\theta}. \tag{62}$$

Substituting (56) and (54) into (48) and taking $\frac{d}{d\epsilon}$ gives

$$\frac{d}{d\epsilon}[0]\big|_{\epsilon=0} = \frac{d}{d\epsilon}\left[\overline{\gamma}_1(0) + \epsilon\hat{\gamma}_1(0)\right]\big|_{\epsilon=0},$$

which simplifies to

$$0 = \hat{\gamma}_1(0).$$

The rest of the boundary conditions are computed similarly giving

$$0 = \hat{\gamma}_1(0) = \hat{\gamma}_1(1) = \hat{\nu}(0) = \hat{\nu}(1). \tag{63}$$

We will drop the hat notation from (58), (59), (61), (62), and (63) giving

$$\theta' = \nu, \tag{64}$$

$$\nu' = -\gamma_1 - B\theta, \tag{65}$$

$$\gamma_1' = Ay, \tag{66}$$

$$y' = \theta, \tag{67}$$

$$0 = \gamma_1(0) = \gamma_1(1) = \nu(0) = \nu(1). \tag{68}$$

Note that the information about the base state is now contained withtin A, see (60).

We can write the system of equations (64), (65), (66), and (67) with matrices as

$$\begin{bmatrix} \theta \\ \nu \\ \gamma_1 \\ y \end{bmatrix}' = \begin{bmatrix} 0 & 1 & 0 & 0 \\ -B & 0 & -1 & 0 \\ 0 & 0 & 0 & A \\ 1 & 0 & 0 & 0 \end{bmatrix} \begin{bmatrix} \theta \\ \nu \\ \gamma_1 \\ y \end{bmatrix}. \tag{69}$$

If we set

$$\begin{bmatrix} \theta \\ \nu \\ \gamma_1 \\ y \end{bmatrix} = X \tag{70}$$

and

$$\begin{bmatrix} 0 & 1 & 0 & 0 \\ -B & 0 & -1 & 0 \\ 0 & 0 & 0 & A \\ 1 & 0 & 0 & 0 \end{bmatrix} = \Lambda, \tag{71}$$

then we can rewrite (69) as

$$X' = \Lambda X. \tag{72}$$

7 Finding Nontrivial Solutions to the Linearized Problem

We want to find combinations of A and B that correspond to nontrival solutions of the 2-point boundary value problem consisting of (68) and (69). Note that A is defined by (60) and F_l and F_u are defined by (53). The combination of these shows that A itself is a function of the parameters ω_1, ω_2, σ_1, σ_2, n_1, n_2, n_3, and n_4. This means that by finding combinations of A and B where (68), (69) has nontrivial solutions we can then find combinations of all the parameters that correspond to non-trivial solutions.

The problem (68), (69) has a general solution $X(s) = e^{\Lambda s}\vec{d}$ where $\vec{d}$ is a vector of arbitrary constants. We get conditions on A and B by enforcing the boundary conditions. First, it is useful to diagonalize Λ and put the matrix exponential in a different form. To do this we find eigenvalues and eigenvectors for Λ. We solve for eigenvalues by solving $det(\Lambda - \lambda I) = 0$, or

$$det\left(\begin{bmatrix} -\lambda & 1 & 0 & 0 \\ -B & -\lambda & -1 & 0 \\ 0 & 0 & -\lambda & A \\ 1 & 0 & 0 & -\lambda \end{bmatrix}\right) = 0. \tag{73}$$

This gives

$$0 = \lambda^4 + B\lambda^2 + A,$$

which has 4 solutions

$$\lambda_1 = \frac{1}{\sqrt{2}}\sqrt{-B + \sqrt{B^2 - 4A}}, \tag{74}$$

$$\lambda_2 = \frac{1}{\sqrt{2}}\sqrt{-B - \sqrt{B^2 - 4A}}, \tag{75}$$

$$\lambda_3 = -\frac{1}{\sqrt{2}}\sqrt{-B + \sqrt{B^2 - 4A}}, \tag{76}$$

and

$$\lambda_4 = -\frac{1}{\sqrt{2}}\sqrt{-B - \sqrt{B^2 - 4A}}. \tag{77}$$

To calculate the eigenvectors we solve $\vec{0} = (\Lambda - \lambda I)\vec{c}$, or

$$\begin{bmatrix} 0 \\ 0 \\ 0 \\ 0 \end{bmatrix} = \begin{bmatrix} -\lambda & 1 & 0 & 0 \\ -B & -\lambda & -1 & 0 \\ 0 & 0 & -\lambda & A \\ 1 & 0 & 0 & -\lambda \end{bmatrix} \begin{bmatrix} c_1 \\ c_2 \\ c_3 \\ c_4 \end{bmatrix}, \tag{78}$$

where λ is one of the 4 values given above. This matrix equation corresponds to

$$0 = -\lambda c_1 + c_2, \tag{79}$$

$$0 = -Bc_1 - \lambda c_2 - c_3, \tag{80}$$

$$0 = -\lambda c_3 + A, \tag{81}$$

and

$$0 = c_1 - \lambda c_4. \tag{82}$$

Choosing $c_4 = 1$ as an initial choice and substituting into (81) and (82) gives $c_3 = \frac{A}{\lambda}$ and $c_1 = \lambda$ respectively. Substitiuting $c_1 = \lambda$ into (79) results in $c_2 = \lambda^2$. Using these new values we can write the eigenvector $\vec{c}$ corresponding to the eigenvalue λ as

$$\vec{c} = \begin{bmatrix} \lambda \\ \lambda^2 \\ \frac{A}{\lambda} \\ 1 \end{bmatrix}. \tag{83}$$

We now introduce two new matrices D and P. D is the diagonal matrix

$$D = \begin{bmatrix} \lambda_1 & 0 & 0 & 0 \\ 0 & \lambda_2 & 0 & 0 \\ 0 & 0 & \lambda_3 & 0 \\ 0 & 0 & 0 & \lambda_4 \end{bmatrix} \tag{84}$$

where λ_1 to λ_4 are given by (74), (75), (76), and (77). P is the matrix whose i^{th} column is the eigenvector

corresponding to the eigenvalue λ_i. So

$$P = \begin{bmatrix} \lambda_1 & \lambda_2 & \lambda_3 & \lambda_4 \\ \lambda_1^2 & \lambda_2^2 & \lambda_3^2 & \lambda_4^2 \\ \frac{A}{\lambda_1} & \frac{A}{\lambda_2} & \frac{A}{\lambda_3} & \frac{A}{\lambda_4} \\ 1 & 1 & 1 & 1 \end{bmatrix}. \tag{85}$$

P^{-1} is found using the adjoint method for finding inverse matrices. This process results in

$$P^{-1} = \frac{1}{-4\lambda_1\lambda_4 + 2\frac{\lambda_1^3}{\lambda_4} + 2\frac{\lambda_4^3}{\lambda_1}} \begin{bmatrix} -\lambda_4 + \frac{\lambda_1^2}{\lambda_4} & -\frac{\lambda_4}{\lambda_1} + \frac{\lambda_1}{\lambda_4} & -\frac{\lambda_4\lambda_1^2+\lambda_4^3}{A} & -\lambda_1\lambda_4 + \frac{\lambda_4^3}{\lambda_1} \\ \lambda_1 - \frac{\lambda_4^2}{\lambda_1} & \frac{\lambda_4}{\lambda_1} - \frac{\lambda_1}{\lambda_4} & \frac{\lambda_1\lambda_4^2-\lambda_1^3}{A} & -\lambda_1\lambda_4 + \frac{\lambda_1^3}{\lambda_4} \\ \lambda_4 - \frac{\lambda_1^2}{\lambda_4} & -\frac{\lambda_4}{\lambda_1} + \frac{\lambda_1}{\lambda_4} & \frac{\lambda_4\lambda_1^2-\lambda_4^3}{A} & -\lambda_1\lambda_4 + \frac{\lambda_4^3}{\lambda_1} \\ -\lambda_1 + \frac{\lambda_4^2}{\lambda_1} & \frac{\lambda_4}{\lambda_1} - \frac{\lambda_1}{\lambda_4} & -\frac{\lambda_1\lambda_4^2+\lambda_1^3}{A} & -\lambda_1\lambda_4 + \frac{\lambda_1^3}{\lambda_4} \end{bmatrix}. \tag{86}$$

We can now rewrite Λ as

$$\Lambda = PDP^{-1},$$

and then we can write $e^{\Lambda s}$ as

$$e^{\Lambda s} = e^{PDP^{-1}s}. \tag{87}$$

We use the power series to write the matrix exponential on the right-hand side of (87) as

$$e^{PDP^{-1}s} = \sum_{n=0}^{\infty} \frac{(PDP^{-1}s)^n}{n!} = I + \frac{(PDP^{-1})^1 s}{1!} + \frac{(PDP^{-1})^2 s^2}{2!} + ...$$

By the properties of matrix multiplication $(PDP^{-1})^n = PD^nP^{-1}$. This means we can write the right hand side of (87) as

$$\begin{aligned} e^{PDP^{-1}s} &= I + P\left(\sum_{n=1}^{\infty} \frac{(Ds)^n}{n!}\right) P^{-1} \\ &= PP^{-1} + P\left(\sum_{n=1}^{\infty} \frac{(Ds)^n}{n!}\right) P^{-1} \\ &= P\left(I + \sum_{n=1}^{\infty} \frac{(Ds)^n}{n!}\right) P^{-1} \end{aligned}$$

$$= P\left(\sum_{n=0}^{\infty} \frac{(Ds)^n}{n!}\right) P^{-1}.$$

Hence

$$e^{\Lambda s} = Pe^{Ds}P^{-1}. \tag{88}$$

By properties of the matrix exponential, we know

$$e^{Ds} = \begin{bmatrix} e^{\lambda_1 s} & 0 & 0 & 0 \\ 0 & e^{\lambda_2 s} & 0 & 0 \\ 0 & 0 & e^{\lambda_3 s} & 0 \\ 0 & 0 & 0 & e^{\lambda_4 s} \end{bmatrix}. \tag{89}$$

The general solution is now

$$X(s) = Pe^{Ds}P^{-1}\vec{d}. \tag{90}$$

Now we enforce the boundary conditions using (90). We will write $Pe^{D}P^{-1}$ as M for easier syntax. By (70) and (90),

$$\begin{bmatrix} \theta(0) \\ \nu(0) \\ \gamma_1(0) \\ y(0) \end{bmatrix} = X(0) = \vec{d} = \begin{bmatrix} d_1 \\ d_2 \\ d_3 \\ d_4 \end{bmatrix}.$$

Equation (68) then tells us that $d_2 = d_3 = 0$. Also,

$$\begin{bmatrix} \theta(1) \\ \nu(1) \\ \gamma_1(1) \\ y(1) \end{bmatrix} = X(1) = M\vec{d} = M \begin{bmatrix} d_1 \\ d_2 \\ d_3 \\ d_4 \end{bmatrix} = \begin{bmatrix} M_1\vec{d} \\ M_2\vec{d} \\ M_3\vec{d} \\ M_4\vec{d} \end{bmatrix},$$

where M_i is the i^{th} row of M. Then from (68) we see that

$$\begin{bmatrix} 0 \\ 0 \end{bmatrix} = \begin{bmatrix} M_2 \vec{d} \\ M_3 \vec{d} \end{bmatrix} = \begin{bmatrix} M_{21}d_1 + M_{24}d_4 \\ M_{31}d_1 + M_{34}d_4 \end{bmatrix} = \begin{bmatrix} M_{21} + M_{24} \\ M_{31} + M_{34} \end{bmatrix} \begin{bmatrix} d_1 \\ d_4 \end{bmatrix}, \tag{91}$$

where the second equality uses that $d_2 = d_3 = 0$. Equation (91) has a nontrivial solution if and only if

$$0 = M_{21}M_{34} - M_{24}M_{31}. \tag{92}$$

Each of the components of M is a function of λ_1 and λ_4. Since λ_1 and λ_4 are functions of A and B we can now use (92) to find combinations of A and B that correspond to non-trivial solutions of (68), (69).

8 Using Matlab to Compute Buckling Loads

The goal in this section is to explain how we find combinations of edge loads B and separations D at which the rod buckles. A first step is to find solutions to (92). Using (74) through (77), (85), (86), and (89) we see that the right-hand side of (92) is a complicated function of A and B. We denote this function by H and use MATLAB to compute H(A, B) numerically. See (A.2). Solutions to (92) correspond to zero values of H. See Figure 5 for the plot of solutions to (92).

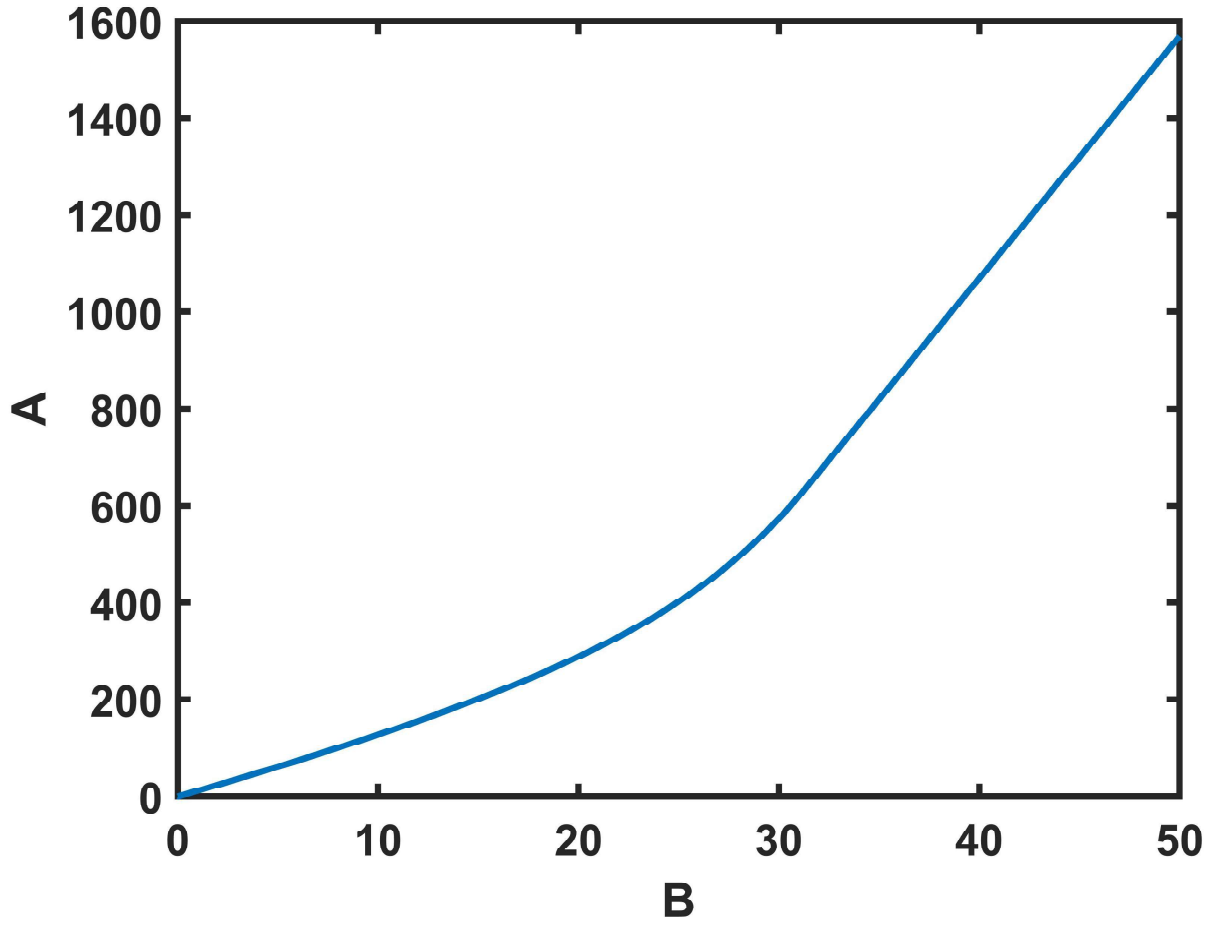

Figure 5: Pairs of edge loads B and A that solve (92).

One can check numerically that H has no zeros above and to the left of the curve in Figure 5. Hence this curve is the set of points (B, A) such that B is the smallest value of B that solves (92) for each A value. Because of this, for a point (B, A) we interpret B as the the buckling load, i.e., as the value of the edge load at which the rod buckles for a fixed A.

To use the data plotted in Figure 5, we can fix the parameters ω_1, ω_2, σ_1, σ_2, n_1, n_2, n_3, and n_4 in (53) and then generate $\overline{y}$ and D pairs that solve (52). A typical plot can be seen in Figure 4.

The plot in Figure 4 shows 3 different branches of equilibrium solutions. We next explain how we compute the buckling load B for a given equilibrium solution. We pick a branch in Figure 4 and pick a point $(\overline{y}, D)$ on the branch. We use the $\overline{y}$ and D values along with fixed values of the other parameters in F_l and F_u to compute a value of A from (60). We then match the A value with a B value using the data plotted in Figure 5. This procedure allows us to generate pairs of edge loads B and substrate separations D corresponding to buckling along a given branch of equilibrium solutions. See Figure 6. Repeating this procedure, we can construct plots like Figure 6 for different choices of the parameters ω_1, ω_2, σ_1, σ_2, n_1, n_2, n_3, and n_4. After that is done, conclusions can be drawn about the system based the change in the graphs that result from the different choices of parameters.

9 Results

In this section we will interpret some of our results physically and we will present and discuss the results generated by the parametric study performed. We will first discuss the results and model when $F_l = F_u$. When performing the parametric study we focus on the effect of varying ω_2 from ω_1. We will focus on leaving all parameters the same and varying the value of ω_2. We will then analyze the plots generated as we did with Figure 4 and will do with Figure 6.

We can use plots such as Figure 4 to determine the postion of the rod between the two substrates when the rod is in an equilibrium configuration. Furthermore, we can use plots such as Figure 6 to observe how much edge load is required to buckle the rod from an equilibrium configuration and to understand how the buckling load depends on the position of the unbuckled rod between the upper and lower substrates.

Recall from Figure 4 that there are three branches of equilibrium solutions. For all the plots that follow, the red branch, branch 2, will always be the branch that approaches the $y = 1$ line which is the branch where the rod is close the the lower substrate. The green branch, branch 3, will always be the branch that approaches the $y = D - 1$ line which is the branch where the rod is close to the upper substrate. The blue branch, branch 1, will always be that branch that is in the resting roughly in the middle of the two substrates. Also, one can check numerically that the part of branch 1 in Figure 4 above and to the right of the branch point is composed of $(\overline{y}, D)$ that in (60) generate an $A < 0$ value. This means the value of B is negative as well. This physically represents that the rod requires tension to maintain stability. We are not interested in this portion of branch 1, and the corresponding portion will not be shown in the buckling load plots.

9.1 Case 1

In this subsection, we set $F_l = F_u$, with $w_1 = w_2 = 1, \sigma_1 = \sigma_2 = 1, n_1 = n_3 = 4$, and $n_2 = n_4 = 2$. Hence the lower and upper substrate have an equivalently strong interaction. The plot of equilibrium configurations corresponding to these parameters is shown in Figure 4.

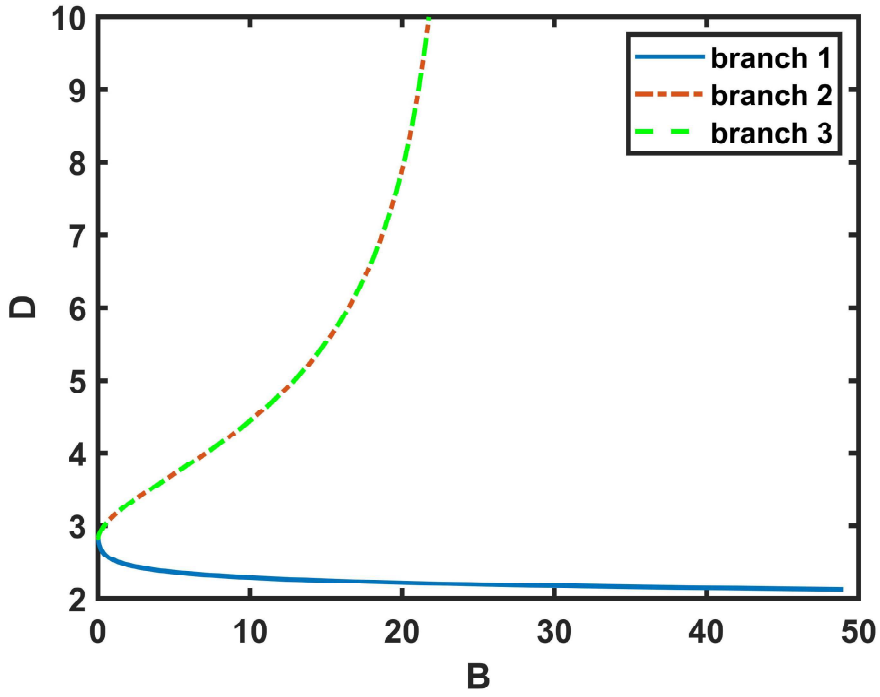

Figure 6: Buckling loads for $F_l = F_u$, with $w_1 = w_2 = 1, \sigma_1 = \sigma_2 = 1, n_1 = n_3 = 4$, and $n_2 = n_4 = 2$.

On branch 1 in Figure 6 we see that as the substrate separation decreases the required buckling load increases. This occurs because of the stronger repulsive interaction forces between from the substrates, which one can think of as squeezing the rod and holding it in the configuration directly between the substrates. A large edge load is necessary to overcome these transverse constraining forces below the branch point. Above the branch point we can see different stories with the branch 2 and 3. As discussed previously, branch 2 approaches $y = 1$ as the substrates separate representing the rod sticking to the lower substrate. Branch 3 approaches the line $y = D - 1$ as the substrates separate representing the rod sticking to the upper substrate. In both of these cases if we look at the corresponding curves on Figure 4 we see that as substrate separation increases the buckling load increases. This larger edge load requirement is due to the rod's stonger interaction with the upper substrate in the case of branch 3 or the lower substrate in the case of the branch 2.

9.2 Case 2

In this subsection, we set $w_1 = 1, w_2 = .9, \sigma_1 = \sigma_2 = 1, n_1 = n_3 = 4$, and $n_2 = n_4 = 2$. Hence the interaction with the upper substrate is slightly weaker than the interaction with the lower substrate.

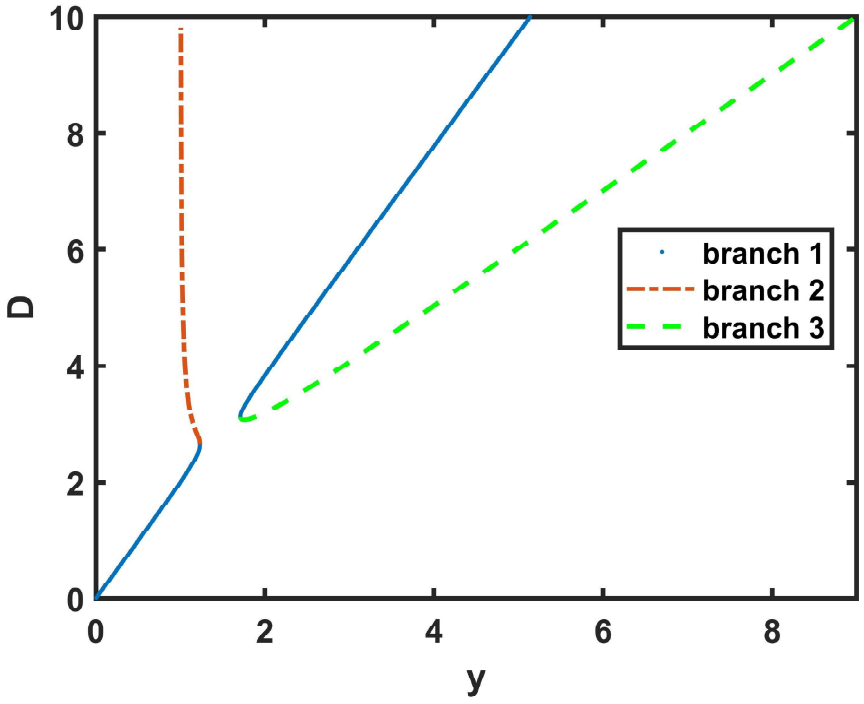

Figure 7: Equilibrium configurations for $w_1 = 1, w_2 = .9, \sigma_1 = \sigma_2 = 1, n_1 = n_3 = 4$, and $n_2 = n_4 = 2$.

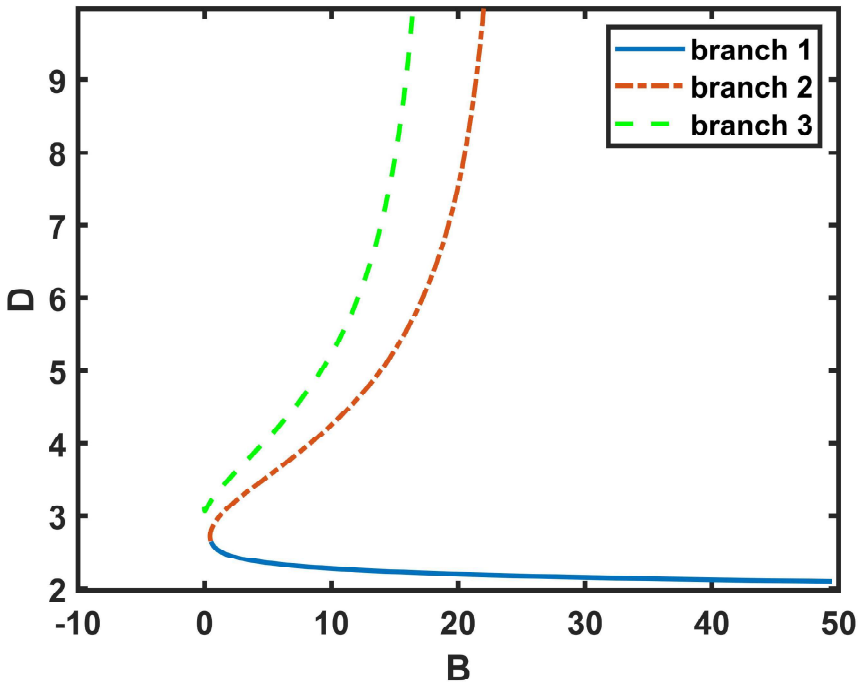

Figure 8: Buckling loads for $w_1 = 1, w_2 = .9, \sigma_1 = \sigma_2 = 1, n_1 = n_3 = 4$, and $n_2 = n_4 = 2$.

The results after reducing ω_2 to 0.9 are shown in Figure 7 and Figure 8. There several differences that we can identify in these. Compared to Figure 4, Figure 7 now has two separate curves. Branch 2 is similar to the branch 2 from Figure 4 as it approaches the line $y = 1$ as substrate separation increases. The lower part of branch 1 generally follows the $y = \frac{1}{2}D$ is slightly steeper meaning it is still close to directly between the substrates but it is now slightly closer to the lower substrate. We can see similar behavior with the upper portion of branch 1. Branch 3 from Figure 7 approaches the line $y = D - 1$ as substrate separation increases showing similarites to the branch 3 from Figure 4. This makes sense as when the substrate separation is large both substrates are pulling the rod toward them but the lower interaction is stronger because $w_1 > w_2$. Alternatively when when the serperation is small the stronger repulsion of the lower substrate pushes the rod closer to the upper substrate.

Observing the number of equilibrium solutions at different substrate separations, we find that at substrate separation below Branch 3 there is only one equilibrium solution. At the Minimum D value of branch 3 there are two equilibrium solutions and at substrate separations higher there are three equilibrium solutions. We will refere to this minimum substrate separation as D_m. This means Figure 7 goes from one configuration to two configurations to three configurations as substrate separation increases. Figure 4 goes from one equilibrium solution directly to three.

Another difference between Figure 6 and Figure 8 is that branch 2 and the branch 3, the branches representing the rod being close to either the upper or the lower substrate, in Figure 4 have the same corresponding buckling loads since the upper and lower interaction forces are the same. Since these forces are no longer the same in Figure 8 there are now different corresponding buckling loads for branch 2 and 3. We can identify that at every substrate separation, branch 2 corresponds to a larger buckling load than branch 3. Branch 1 from Figure 7 and their corresponding plots on Figure 8 are nearly the same as branch 1 from Figure 4. The main difference is that branch 1 from Figure 7 splits into branch 2 at a smaller substrate separation. This occurs because the rod sticks to the lower substrate at a smaller substrate separation. In Figure 7 not every y value has a corresponding substrate separation that gives an equilibrium solution. Specifically there is an interval between $y = 1$ and $y = 2$ where there are no corresponding equilibrium solutions.

9.3 Case 3 and 4

For Case 3, we set $w_1 = 1, w_2 = .5, \sigma_1 = \sigma_2 = 1, n_1 = n_3 = 4$, and $n_2 = n_4 = 2$. Hence the interaction with the upper substrate is weaker than the interaction with the lower substrate. See Figures 9

and 10.

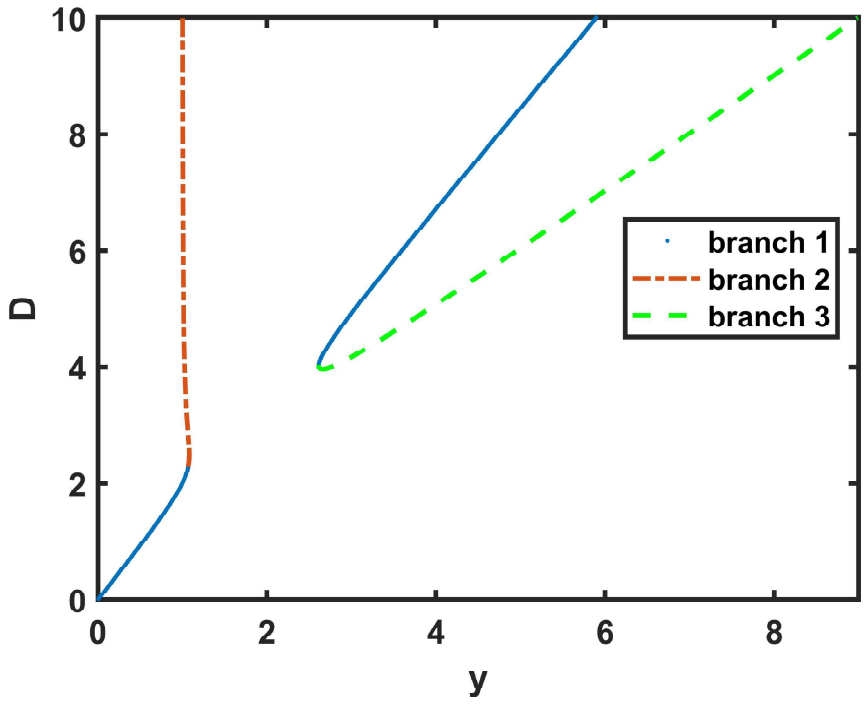

Figure 9: Equilibrium configurations for $w_1 = 1, w_2 = .5, \sigma_1 = \sigma_2 = 1, n_1 = n_3 = 4$, and $n_2 = n_4 = 2$.

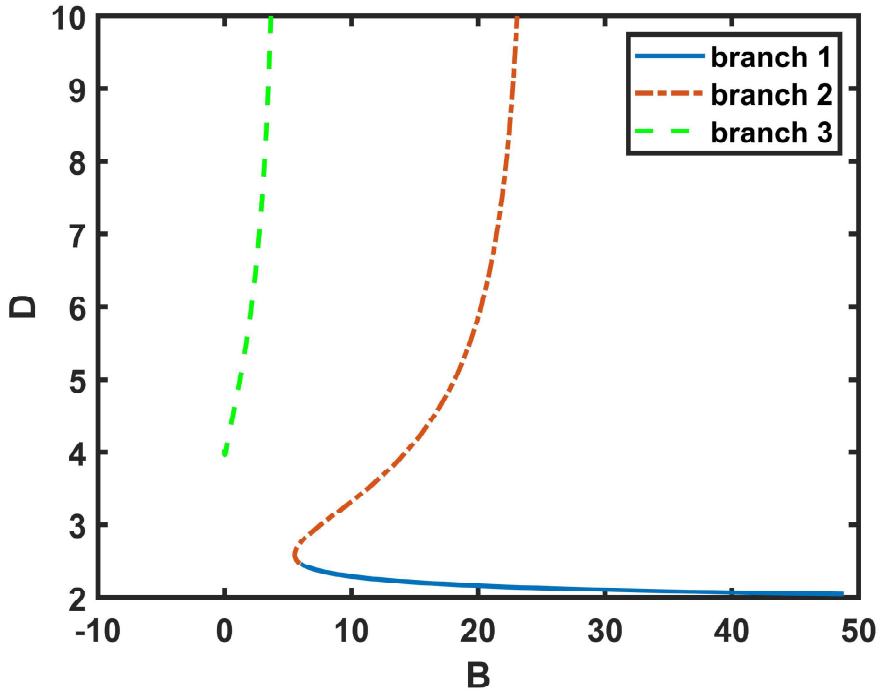

Figure 10: Buckling loads for $w_1 = 1, w_2 = .5, \sigma_1 = \sigma_2 = 1, n_1 = n_3 = 4$, and $n_2 = n_4 = 2$.

For Case 4, we set $w_1 = 1, w_2 = .2, \sigma_1 = \sigma_2 = 1, n_1 = n_3 = 4$, and $n_2 = n_4 = 2$. Hence the interaction with the upper substrate is much weaker than the interaction with the lower substrate See Figures 11 and 12

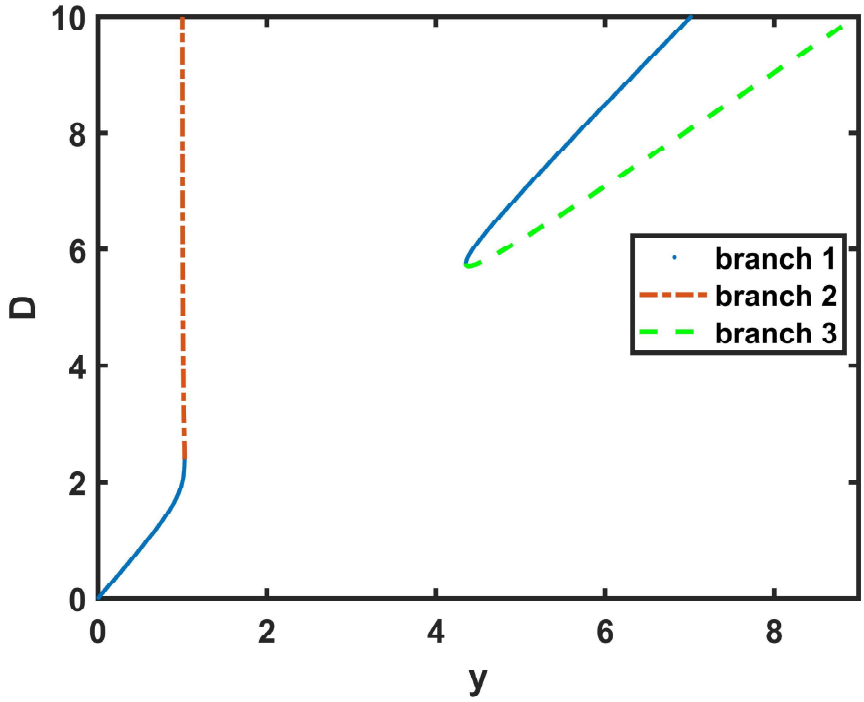

Figure 11: Equilibrium configurations for $w_1 = 1, w_2 = .2, \sigma_1 = \sigma_2 = 1, n_1 = n_3 = 4$, and $n_2 = n_4 = 2$.

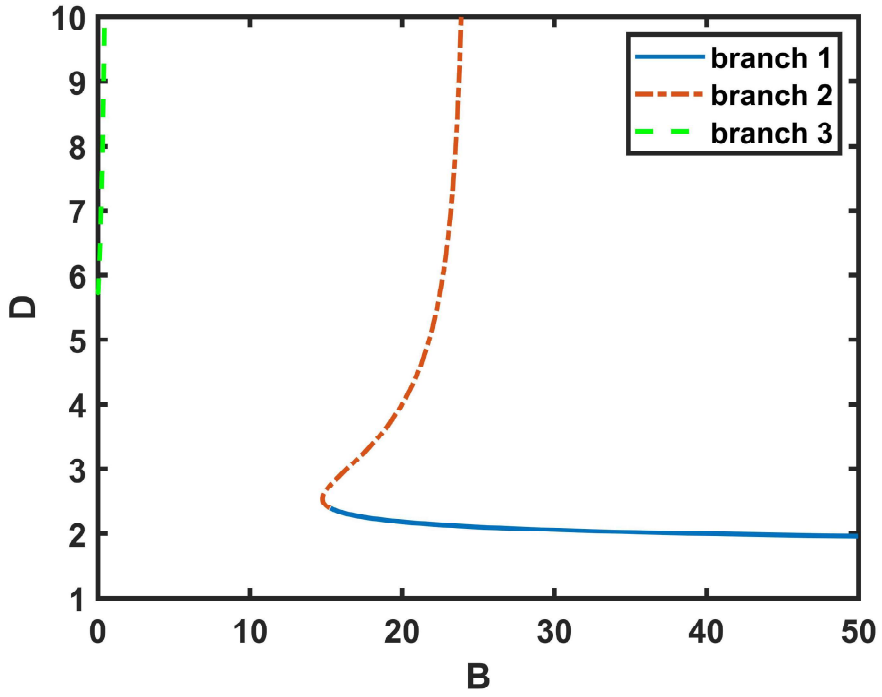

Figure 12: Buckling loads for $w_1 = 1, w_2 = .2, \sigma_1 = \sigma_2 = 1, n_1 = n_3 = 4$, and $n_2 = n_4 = 2$.

We will not decrease ω_2 any further as branch 3 becomes difficult to resolve numerically on the buckling load plots. Figure 9 and Figure 11 illustrate similar behavior to that seen in Figure 7. Figure 10, and Figure 12 also show similar behavior to what we see in Figure 8. This similarity makes sense because the system has not qualitatively changed in cases 2, 3, and 4. As ω_2 becomes much smaller than ω_1 the length of the y values for which there are no substrate separations increases. In Figure 9 this length has increased to approximately 1.5 units. In Figure 12 it further increases to approximately three units. As ω_2 becomes much smaller than ω_1 the minimim buckling load on branch 2 for Figure 12, Figure 10, and Figure 8 increases. In Figure 8 the minimum buckling load on branch 2 is near zero and in Figure 12 it is nearly 15. The buckling loads for branch 3, the configuration that is close to the upper substrate, are decreasing as we decrease ω_2.

9.4 Case 5 and 6

For Case 5, we set $w_1 = 1, w_2 = 1.1, \sigma_1 = \sigma_2 = 1, n_1 = n_3 = 4$, and $n_2 = n_4 = 2$. Hence the interaction with the upper substrate is slightly stronger than the interaction with the lower substrate. See Figures 13 and 14.

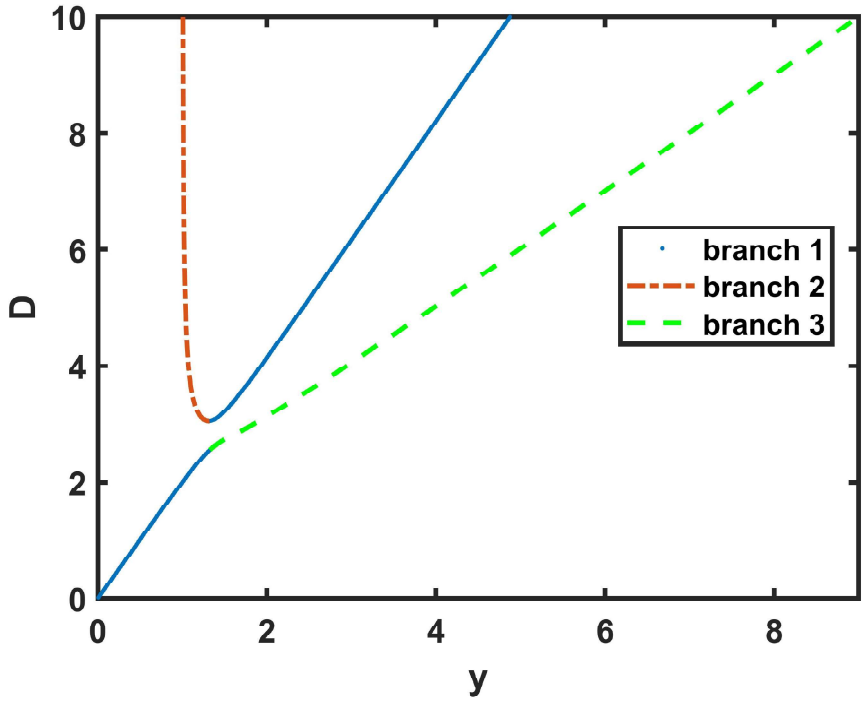

Figure 13: Equilibrium configurations for $w_1 = 1, w_2 = 1.1, \sigma_1 = \sigma_2 = 1, n_1 = n_3 = 4$, and $n_2 = n_4 = 2$.

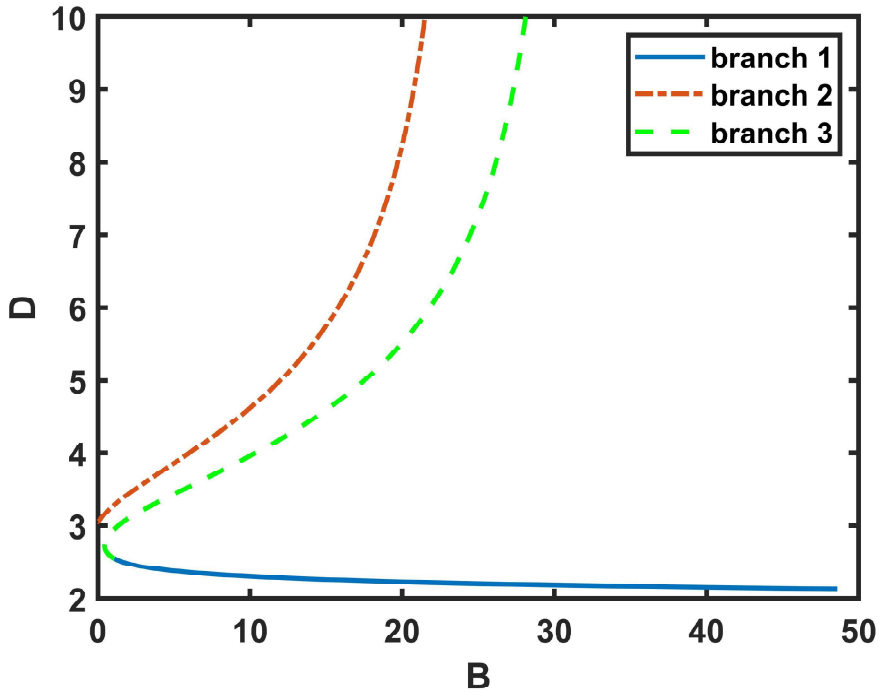

Figure 14: Buckling loads for $w_1 = 1, w_2 = 1.1, \sigma_1 = \sigma_2 = 1, n_1 = n_3 = 4$, and $n_2 = n_4 = 2$.

For Case 6, we set $w_1 = 1, w_2 = 2, \sigma_1 = \sigma_2 = 1, n_1 = n_3 = 4$, and $n_2 = n_4 = 2$. Hence the interaction with the upper substrate is much stronger than the interaction with the lower substrate. See Figures 15 and 16.

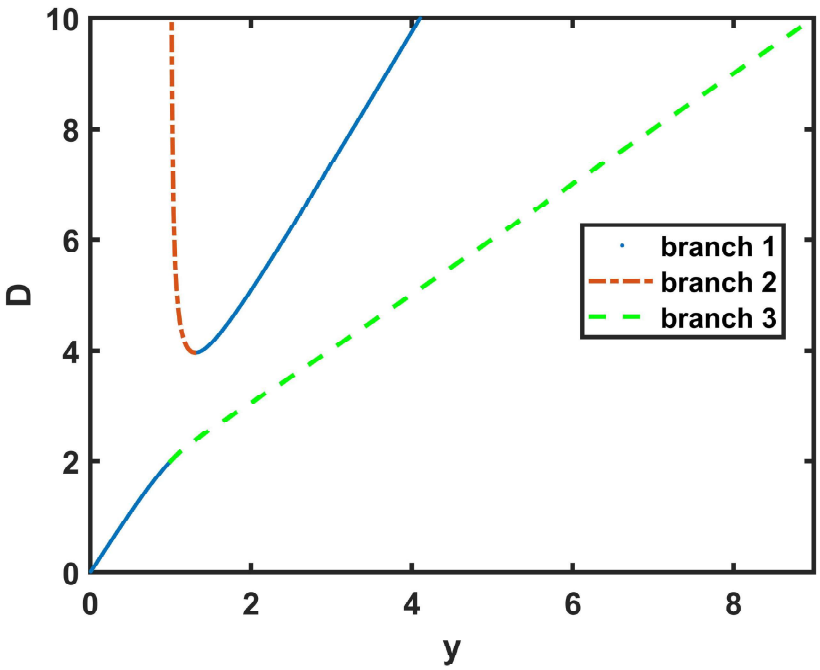

Figure 15: Equilibrium configurations for $w_1 = 1, w_2 = 2, \sigma_1 = \sigma_2 = 1, n_1 = n_3 = 4$, and $n_2 = n_4 = 2$.

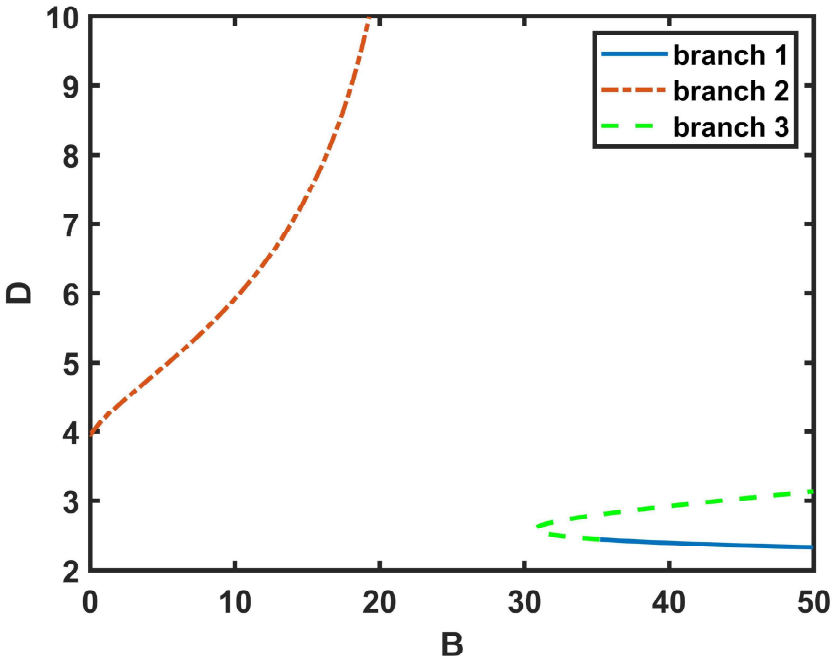

Figure 16: Buckling loads for $w_1 = 1, w_2 = 2, \sigma_1 = \sigma_2 = 1, n_1 = n_3 = 4$, and $n_2 = n_4 = 2$.

In Figure 14 and Figure 16 the configurations that require the larger edge load to buckle is now branch 3. The required buckling load for those configurations also increases as ω_2 increases. This makes sense as the attractive force pulling the rod to the substrate is greater with a larger ω meaning it takes a larger load to overcome. Case 5 and 6 are qualitatively opposite to Cases 2, 3, and 4 because now $\omega_2 > \omega_1$. This means our explanation for these the results for Case 2 holds but toward the opposite substrate. We will not further increase ω_2 beyond 2 as branch 1 and 3 become larger than the B values we interpolated in Figure 5.

10 Conclusions

Using Figure 4 through Figure 16 we look at the general effect of different ω values on the predictions of the model. We can see the from the equilibrium configuration graphs that there are three branches of configurations, one sticking to the lower substrate, one sticking to the upper substrate, and one held exactly or approximately in the middle of the substrates. From Figure 4 it is evident that when the upper interaction and lower interaction are equal the rod rests directly halfway between the substrates. As ω_2 decreases we can identify from Figure 12 that at large separations between the substrates this middle configuration rests closer to the lower substrate when ω_2 is smaller. From Figure 16 the opposite is present as the branch 1 configuration rests closer to the upper substrate when ω_2 is larger. Since ω_2 is associated with the upper interaction it appears that the branch 1 configuration rests closer substrate with the larger ω. The buckling loads required for branch 1 seem to show a similar behavior in the range of ω values considered. In all the buckling load plots, when the substrate separation is small the edge load required is large and at large substrate separations the edge load required is nearly 0. This is likely due to the larger interference from the substrates preventing the rod from buckling at smaller seperation. The ω values seem to have more of an effect on the range of y values in branch 1 and on the specific substrate separation D at which branch 2 or 3 splits from branch 1. Branch 1 will tend toward the substrate with the smaller corresponding ω and will split toward the branch that is associated with the larger ω at a smaller substrate separation D.

For the branches with configurations that stick to one of the substrates, the edge load required to buckle the rod is different depending on which substrate the rod is sticking to. When ω_2 is smaller the rod needs less load to buckle when it is sticking to the upper substrate and more load to buckle when it is sticking to the lower substrate. This can bee seen in Figure 8, Figure 10, and Figure 12. When ω_2 is larger the opposite is true, which can be seen in Figure 14 and Figure 16. This indicates that when the rod is sticking to the substrate with the larger ω, it requires more edge load to buckle than when the rod is sticking to the other substrate. This is consistent with the idea that ω measures the strength of the interaction. This means the rod requires a larger edge load to buckle when the rod is sticking to the substrate with the stronger interaction force.

When ω_2 is larger or smaller than ω_1 the smallest D value where the rod will stick to the substrate with smaller ω is at a larger substrate separation D. From Figure 8, Figure 10, and Figure 12, we see that branch 3 begins at a larger substrate separation as ω_2 gets smaller. This can also be seen in in Figure 14

and Figure 16, as branch 2 begins at a larger substrate separation D as ω_2 gets larger. This likely occurs because the rod, for relatively smaller substrate separations, can not get far enough away from the stronger interaction to be at equilibrium in the branch 2 configuration, which is the configuration sticking to the substrate with the lower ω value. This can also explain the intervals of y values where for which there are no equilibrium configurations, as is seen in Figure 7, Figure 9, and Figure 11. In these figures we see that the larger constraining force is causing the rod to be forced into the branch 2 configuration. This means at the substrate separations where the rod would equilibrate in the branch 1 configuration or the branch 3 configuration close to the top, it is not able. Once the substrate separation is large enough, the rod can attain the branch 3 equilibrium configuration. This does not occur when ω_2 is larger, as seen in Figure 13 and Figure 15. As the substrate separation increases, the rod goes from branch 1, between the substrates to sticking to the top substrate. This means as the substrate separation increases, the vertical position of the rod increases with it. Hence every vertical position has a substrate separation for which there is an equilibrium solution.

A MATLAB Code

A.1 $F_l - F_u$

```
function FlFu = AFunc(w1, sigma1, n1, n2, w2, sigma2, n3, n4)
%upper substrate parameters
w1 = 1;
sigma1 = 1;
n1 = 4;
n2 = 2;
%lower substrate parameters
w2 = 2;
sigma2 = 1;
n3 = 4;
n4 = 2;

d = linspace(0,10,2000);
y = linspace(0,10,2000);

[Y,D]= meshgrid(y,d);

F = w1.*((sigma1./Y).^n1 - (sigma1./Y).^n2) - w2.*((sigma2./(D-Y)).^n3 - (sigma2./(D-Y
    )).^n4);

L = contour(Y,D,F,[0 0]); %produces a plot with values of y and D that satisfy 0 = Fl
    - Fu
end
```

A.2 $Hfunc$

```
function H = Hfunc(B,A)
%calculates the values for Lambdas for given A and B
 La1 = (1/sqrt(2)).*sqrt(-1.*B + sqrt(B.^2-(4.*A)));
 La2 = (1/sqrt(2)).*sqrt(-1.*B - sqrt(B.^2-(4.*A)));
 La3 = -(1/sqrt(2)).*sqrt(-1.*B + sqrt(B.^2-(4.*A)));
 La4 = -(1/sqrt(2)).*sqrt(-1.*B - sqrt(B.^2-(4.*A)));

%calculates a value used to compute the hand derived P-inverse Matrix
 star = ((-4 .* La1 .* La4) + (2 .* La1.^3 ./ La4) + (2 .* La4.^3 ./ La1));

%calculates P Matrix
P = [(La1) (La2) (La3) (La4);
    (La1.^2) (La2.^2) (La3.^2) (La4.^2);
    (A./La1) (A./La2) (A./La3) (A./La4);
    1 1 1 1];

%row 1 of P inverse
Pv11 = ((-1.*La4 + La1.^2 ./La4)./star);
Pv12 = (((-1.*La4./La1)+(La1./La4))./(star));
```

```
Pv13 = ((-1.*La4 .* La1.^2 + La4.^3)./ (A.*star));
Pv14 = ((-1.*La1.*La4 + La4.^3 ./La1) ./(star));

%row 2 of P inverse
Pv21 = ((La1 + -1.*La4.^2 ./La1)./star);
%Pv22 = -Pv12; -----Doesn't need to be calculated
Pv23 = ((La1 .* La4.^2 + -1.*La1.^3)./ (A.*star));
Pv24 = ((-La1.*La4 + La1.^3 ./ La4) ./(star));

%find the P inverse matrix
%Pinv = inv(P);
Pinv = [Pv11 Pv12 Pv13 Pv14;
          Pv21 -Pv12 Pv23 Pv24;
          -Pv11 Pv12 -Pv13 Pv14;
          -Pv21 -Pv12 -Pv23 Pv24];

%find the diagonal matrixd
eD = [exp(La1) 0 0 0;
      0 exp(La2) 0 0;
      0 0 exp(La3) 0;
      0 0 0 exp(La4)];

%finds the M Matrix
M = P * eD * Pinv;

%uses formula (91)
H = abs(M(2,1).*M(3,4) - M(2,4).*M(3,1));
end
```

A.3 *trackingLowerMinWithA*

```
% this creates a graph on the B and A axes given a range of A values and density
    points.
% B(horizontal axis), (A vertical axis)

s=2500;    %size of matrix rows and columns
Bmin = 0;  %minimum value of A
Bmax = 50; %maximum value of A


if (Bmin * 12.7) <= 5
   searchMin = 0;  %lower bound is 0 if Amin is 10 or less
else
    searchMin = Bmin * 12.7 -5;  %lower bound when searching for first 0
end
searchMax = Bmin * 12.7 +5; % upper bound when searching for first 0


B= linspace(Bmin,Bmax,s);    % A vector
```

```
18
19 H = zeros(s,1);   % H vector. Starts empty used to find o in a given B interval
20 Amin = zeros(s,1);% B Vector
21 dummy=0;
22 I=0;
23
24 i=1; %this loops is used to find the first 0
25 A = linspace(searchMin,searchMax,s); %first interval for finding 0
26 %A = linspace(0,3,s);
27 for j=1:s
28             H(j)= Hfunc(B(i),A(j));
29 end
30 [dummy , I] = min(H); % dummy is the value of the min, I is the index of min
31  Amin(1) = A(I);       % assigns the value of the B value that gives the lowest H
32
33  i=2;
34  A = linspace(searchMin+.3,searchMax,s);
35  for j=2:s
36             H(j)= Hfunc(B(i),A(j));
37 end
38 [dummy , I] = min(H);  % dummy is the value of the min, I is the index of min
39  Amin(1) = A(I);        % assigns the value of the B value that gives the lowest H
40
41
42
43  slope = ((Bmax- Bmin)/s)*50; %determines the interval in which to check for the next
        0
44
45  %this loops is used to find the rest of the 0's
46 for i=3:s
47  A = linspace(Amin(i-1),Amin(i-1)+slope,s);  %for finding lower zero
48     for j=1:s
49             H(j)= Hfunc(B(i),A(j));
50     end
51  [dummy , I] = min(H);   % dummy is the value of the min, I is the index of min
52  Amin(i) = A(I);         % assigns the value of the B value that gives the lowest H
53 end
54
55 plot(B,Amin,'.')         % plots the 0 on the B and A axes
56
57 BAtakesA = csapi(Amin,B);% makes interpolated function using A and B values determined
       here
```

A.4 *Lplot*

```
1 %Lplot is used to plot the Y and D values that correspond to 0 values of
2 %Fl-Fu
3
4 % used to change paramaters of Fl and Fu
```

```
w1 = 1;
sigma1 = 1;
n1 = 4;
n2 = 2;
w2 = .5;
sigma2 = 1;
n3 = 4;
n4 = 2;

d = linspace(0,10,2000);
y = linspace(0,10,2000);

[Y,D]= meshgrid(y,d);

%F is used for Fl-Fu
F = w1.*((sigma1./Y).^n1 - (sigma1./Y).^n2) - w2.*((sigma2./(D-Y)).^n3 - (sigma2./(D-Y
    )).^n4);

L=contour(Y,D,F, [0 0]); %graphs when F is 0

contourTable = getContourLineCoordinates(L);%collects the Y and D coordinates from the
    contour
%credit (Adam Danz (2021). getContourLineCoordinates
%(https://www.mathworks.com/matlabcentral/fileexchange/74010-getcontourlinecoordinates
    ), MATLAB Central File Exchange. Retrieved November 13, 2021.)

coordinates=table2array(contourTable);%turns the collected coordinates from a table to
    an array

s=size(coordinates,1);

newY=zeros(s,1); %Y will need to be resized to remove the YD pairs not in the model
newD=zeros(s,1); %D will need to be resized to remove the YD pairs not in the model
```

A.5 *adjustLplotCustom*

```
%removes the YD pairs not in the model such as when D is larger than Y
Break1=1;
Break2=772;
Break3=3794;
Break4=7393;
Break5=9492;
Break6=10946;
%%%%%%%%%%%%%%%%%%%%%%%%%%%%%%%%%%%%%%%%%%%%%%%%%%%%%%%%%%%%%%%%%%% keep

% for i=1:Break1  %1st
%       newY(i)= coordinates(i,3);
%       newD(i)= coordinates(i,4);
% end
```

```
14
15 % for i=Break1+1:Break2   %2nd
16 %       newY(i)= coordinates(i,3);
17 %       newD(i)= coordinates(i,4);
18 % end
19
20 % for i=Break2+1:Break3   %3rd
21 %       newY(i)= coordinates(i,3);
22 %       newD(i)= coordinates(i,4);
23 % end
24
25 % for i=Break3+1:Break4   %4th
26 %       newY(i)= coordinates(i,3);
27 %       newD(i)= coordinates(i,4);
28 % end
29
30 % for i=Break4+1:Break5   %5th
31 %       newY(i)= coordinates(i,3);
32 %       newD(i)= coordinates(i,4);
33 % end
34
35 % for i=Break5+1:Break6:   %6th
36 %       newY(i)= coordinates(i,3);
37 %       newD(i)= coordinates(i,4);
38 % end
39
40
41
42 %%%%%%%%%%%%%%%%%%%%%%%%%%%%%%%%%%%%%%%%%%%%%%%%%%%%%%%%%%%%%%%%%% remove
43 for i=Break6:-1:Break5+1 %6th
44       newY(i)=[];
45       newD(i)=[];
46 end
47
48 for i=Break5:-1:Break4+1 %5th
49       newY(i)=[];
50       newD(i)=[];
51 end
52
53 for i=Break4:-1:Break3+1    %4th
54       newY(i)= [];
55       newD(i)= [];
56 end
57
58 for i=Break3:-1:Break2+1    %3rd
59       newY(i)= [];
60       newD(i)= [];
61 end
```

```
62
63 for i=Break2:-1:Break1+1  %2nd
64     newY(i)= [];
65     newD(i)= [];
66 end
67
68 for i=Break1:-1:1  %1st
69     newY(i)= [];
70     newD(i)= [];
71 end
72
73 % for i=1:Break1 %1st
74 %       newY(i)= coordinates(i,3);
75 %       newD(i)= coordinates(i,4);
76 % end
77 % j=Break3+1;
78 %
79 % for i=Break4:-1:Break3+1  %4th
80 %       newY(j)= coordinates(i,3);
81 %       newD(j)= coordinates(i,4);
82 %       j=j+1;
83 % end
84 %%%%%%%%%%%%%%%%%%%%%%%%%%%%%%%%%%%%%%%%%%%%%%%%%%%%%%%%%%%%%%%%%%%%%%%%%%%%
85
86 %for plotting results
87 %plot(newY,newD,'.')
88 plot(newY,newD)
```

A.6 *BD2*

```
1  % makes a plot of B and D values corresponding to buckling
2  % used to change paramaters of A should match the parameters in Lplot
3  w1 = 1;
4  sigma1 = 1;
5  n1 = 4;
6  n2 = 2;
7  w2 = 2;
8  sigma2 = 1;
9  n3 = 4;
10 n4 = 2;
11
12 %newY and NewD found in different file
13
14 s=size(newY,1);
15
16 A=zeros(s,1);
17
18 %generates A values using the Y and D pairs from adjustLplot
19 for i=1:s
```

```
    A(i)=AFunc2(newD(i),newY(i),w1,w2,sigma1,sigma2,n1,n2,n3,n4);
end

B = zeros(s,1);

%finds A value in interpolated BA function and inserts the associated B
%value into B
for i=1:s
    B(i)=fnval(BAtakesA,A(i));
end

%f2=figure; %used to plot multiple graphs

for i=s:-1:1
    if B(i)>50 %ensures values is not larger than interpolated values
    B(i)=[];
    newD(i)=[];
    end
end

%f3=figure; %used to plot multiple graphs

plot(B,newD,'--')
%plot(B,newD)        %used to plot multiple graphs
%plot(B,newD,'-.')  %used to plot multiple graphs
```

A.7 *AFunc2*

```
function A = AFunc2(D,Y,w1,w2,sigma1,sigma2,n1,n2,n3,n4)

A= w1./(Y) .*((n2.*(sigma1./(Y)).^n2) - n1.*(sigma1./(Y)).^n1) +w2./(D-Y).*((n4.*(
    sigma2./(D-Y)).^n4) - n3.*(sigma2./(D-Y)).^n3);

end
```

References

[1] H. W. Kroto, J. R. Heath, S. C. O'Brien, R. F. Curl, and R. E. Smalley. C60: Buckminsterfullerene. *Nature*, 318(6042):162–163, November 1985.

[2] Carbon nanotube — Properties & Uses — Britannica. https://www.britannica.com/science/carbon-nanotube.

[3] P. M. Ajayan and Sumio Lijima. Smallest carbon nanotube. *Nature*, 358(6381):23–23, July 1992. Bandiera_abtest: a Cg_type: Nature Research Journals Number: 6381 Primary_atype: Research Publisher: Nature Publishing Group.

[4] Sumio Iijima and Toshinari Ichihashi. Single-shell carbon nanotubes of 1-nm diameter. *Nature*, 363(6430):603–605, June 1993. Bandiera_abtest: a Cg_type: Nature Research Journals Number: 6430 Primary_atype: Research Publisher: Nature Publishing Group.

[5] D. S. Bethune, C. H. Kiang, M. S. de Vries, G. Gorman, R. Savoy, J. Vazquez, and R. Beyers. Cobalt-catalysed growth of carbon nanotubes with single-atomic-layer walls. *Nature*, 363(6430):605–607, June 1993. Bandiera_abtest: a Cg_type: Nature Research Journals Number: 6430 Primary_atype: Research Publisher: Nature Publishing Group.

[6] null Thess, null Lee, null Nikolaev, null Dai, null Petit, null Robert, null Xu, null Lee, null Kim, null Rinzler, null Colbert, null Scuseria, null Tomanek, null Fischer, and null Smalley. Crystalline Ropes of Metallic Carbon Nanotubes. *Science (New York, N.Y.)*, 273(5274):483–487, July 1996.

[7] C. Journet, W. K. Maser, P. Bernier, A. Loiseau, M. Lamy de la Chapelle, S. Lefrant, P. Deniard, R. Lee, and J. E. Fischer. Large-scale production of single-walled carbon nanotubes by the electric-arc technique. *Nature*, 388(6644):756–758, August 1997. Bandiera_abtest: a Cg_type: Nature Research Journals Number: 6644 Primary_atype: Research Publisher: Nature Publishing Group.

[8] M. S. Dresselhaus, G. Dresselhaus, P. C. Eklund, and A. M. Rao. Carbon Nanotubes. In Wanda Andreoni, editor, *The Physics of Fullerene-Based and Fullerene-Related Materials*, Physics and Chemistry of Materials with Low-Dimensional Structures, pages 331–379. Springer Netherlands, Dordrecht, 2000.

[9] J. Patrick Wilber. Buckling of Graphene Layers Supported by Rigid Substrates. *arXiv:1002.0724 [cond-mat]*, February 2010. arXiv: 1002.0724.

[10] C. Bower, R. Rosen, L. Jin, Jin-Woo Han, and O. Zhou. Deformation of carbon nanotubes in nanotube–polymer composites. 1999.

[11] M. R. Falvo, G. J. Clary, R. M. Taylor, V. Chi, F. P. Brooks, S. Washburn, and R. Superfine. Bending and buckling of carbon nanotubes under large strain. *Nature*, 389(6651):582–584, October 1997.

[12] Eric Wong, Paul Sheehan, and Charles Lieber. Nanobeam Mechanics: Elasticity, Strength, and Toughness of Nanorods and Nanotubes. *Science*, 277:1971–1975, September 1997.

[13] M. M. J. Treacy, T. W. Ebbesen, and J. M. Gibson. Exceptionally high Young's modulus observed for individual carbon nanotubes. *Nature*, 381(6584):678–680, June 1996. Bandiera_abtest: a Cg_type: Nature Research Journals Number: 6584 Primary_atype: Research Publisher: Nature Publishing Group.

[14] Sumio Iijima, Charles Brabec, Amitesh Maiti, and Jerzy Bernholc. Structural flexibility of carbon nanotubes. *The Journal of Chemical Physics*, 104(5):2089–2092, February 1996. Publisher: American Institute of Physics.

[15] J. Scott Bunch, Arend M. van der Zande, Scott S. Verbridge, Ian W. Frank, David M. Tanenbaum, Jeevak M. Parpia, Harold G. Craighead, and Paul L. McEuen. Electromechanical Resonators from Graphene Sheets. *Science*, 315(5811):490–493, January 2007. Publisher: American Association for the Advancement of Science Section: Report.

[16] Doron Gazit. Theory of the spontaneous buckling of doped graphene. *Physical Review B*, 79(11):113411, March 2009. Publisher: American Physical Society.

[17] A. Deshpande, W. Bao, F. Miao, C. N. Lau, and B. J. LeRoy. Spatially resolved spectroscopy of monolayer graphene on SiO_2. *Physical Review B*, 79(20):205411, May 2009. Publisher: American Physical Society.

[18] Kevin R. Knox, Shancai Wang, Alberto Morgante, Dean Cvetko, Andrea Locatelli, Tevfik Onur Mentes, Miguel Angel Niño, Philip Kim, and R. M. Osgood. Spectromicroscopy of single and multilayer graphene supported by a weakly interacting substrate. *Physical Review B*, 78(20):201408, November 2008. Publisher: American Physical Society.

[19] Eun-Ah Kim and A. H. Castro Neto. Graphene as an electronic membrane. *EPL (Europhysics Letters)*, 84(5):57007, December 2008.

[20] Xuekun Lu, Minfeng Yu, Hui Huang, and Rodney S. Ruoff. Tailoring graphite with the goal of achieving single sheets. Nanotechnology, 1999.

[21] H.-V. Roy, C. Kallinger, B. Marsen, and K. Sattler. Manipulation of graphitic sheets using a tunneling microscope. *Journal of Applied Physics*, 83(9):4695–4699, May 1998. Publisher: American Institute of Physics.

[22] Jianfeng Zhou, Ziyong Shen, Shimin Hou, Xingyu Zhao, Zengquan Xue, Zujin Shi, and Zhennan Gu. Adsorption and manipulation of carbon onions on highly oriented pyrolytic graphite studied with atomic force microscopy. *Applied Surface Science*, 253(6):3237–3241, January 2007.

[23] Zhijie Jia, Zhengyuan Wang, Cailu Xu, Ji Liang, Bingqing Wei, Dehai Wu, and Shaowen Zhu. Study on poly(methyl methacrylate)/carbon nanotube composites. *Materials Science & Engineering A*, 1-2(271):395–400, 1999.

[24] Xiaohua Chen, Jintong Xia, Jingcui Peng, Wenzhu Li, and Sishen Xie. Carbon-nanotube metal-matrix composites prepared by electroless plating. *Composites Science and Technology*, 60:301–306, February 2000.

[25] H. D. Wagner, O. Lourie, Y. Feldman, and R. Tenne. Stress-induced fragmentation of multiwall carbon nanotubes in a polymer matrix. *Applied Physics Letters*, 72(2):188–190, January 1998. Publisher: American Institute of Physics.

[26] Erik T Thostenson, Zhifeng Ren, and Tsu-Wei Chou. Advances in the science and technology of carbon nanotubes and their composites: a review. *Composites Science and Technology*, 61(13):1899–1912, October 2001.

[27] Sangjae Seo and Wataru Shinoda. Molecular dynamics simulations. 2018.